Chapter ###

DRAFT DRAFT DRAFT

A Component-Wise Approach in Structural Analysis

E. Carrera, A. Pagani,
M. Petrolo and E. Zappino
Department of Mechanical and Aerospace Engineering
Politecnico di Torino, Italy

Abstract

Many engineering structures can be seen as multicomponent structures. Typical examples of such structures are aircraft wings and fibre-reinforced composites. The former are typically composed of skins, spars, stringers and ribs. The latter are composed by plies made of fibres and matrices. Models built by means of an arbitrary combination of different components lead to a component-wise (CW) analysis. The present chapter presents an innovative CW approach based on the one-dimensional Carrera unified formulation (CUF). The CUF has been developed recently, different classes of models are available and, in this work, Taylor-like (TE) and Lagrange-like (LE) elements were adopted. Different numerical examples are proposed, including aircraft structures, composite laminates and typical buildings from civil engineering. Comparisons with results from solid and shell finite elements are given. It is concluded that the present CW approach represents a reliable and computationally cheap tool which can be exploited for many types of structural analyses.

Keywords: refined beam theories, finite elements, unified formulation, composites, reinforced shell structures, civil engineering structures, component-wise.

1 Introduction

Beam theories are important tools for structural analysts. Interest in beam models is mainly as a result of their simplicity and their low computational costs when compared to two-dimensional (plate or shell) or three-dimensional (solid) models. The classical and best-known beam theories are those by Euler [1], hereinafter referred to as EBBT, and Timoshenko [2,3], hereinafter referred to as TBT. The former does not account for transverse shear deformations. The latter foresees a uniform shear distribution along the cross-section of the beam. These models work properly when slender compact

homogeneous structures are considered in bending. The relevance of a beam theory increases to a great extent if higher-order models are developed to which plate or shell capabilities can be assigned, such as those in [4] and [5].

This work is embedded in the framework of the one-dimensional Carrera unified formulation (CUF) for beam structures. The CUF is a hierarchical formulation which considers the order of the theory as an input of the analysis. This allows us to deal with a wide variety of problems with no need for *ad hoc* formulations. In fact, the governing equations are expressed in terms of a few 'fundamental nuclei' whose form does not depend on the order of the introduced approximations. According to the latest developments on CUF, Lagrange-type polynomials are used to interpolate the displacement field above the cross-section of the beam [6]. The choice of this kind of expansion function leads us to have displacement variables only. Three- (L3), four- (L4), and nine-point (L9) polynomials are considered in the framework of CUF; this leads to linear, quasi-linear (bilinear), and quadratic displacement field approximations over the beam cross-section. More refined beam models are implemented by introducing further discretisations over the beam cross-section in terms of implemented elements. The resulting one-dimensional models can deal with *component-wise* (CW) analysis of multicomponent structures.

Several structures can be considered as multicomponent structures, such as aeronautical structures, fibre-reinforced composites and civil buildings. The former are essentially reinforced thin shells, composed by three main components: panels, longitudinal stiffeners and ribs. Many different approaches for the analysis of aircraft structures were developed in the first half of the last century. These are discussed in major reference books [7, 8] and more recently in [9]. Resulting from the advent of computational methods, mostly finite element method (FEM), the analysis of complex aircraft structures continued to be carried out using a combination of solids (three-dimensional), plates/shells (two-dimensional) and beams (one-dimensional). Nowadays FEM models with a number of unknowns (degrees of freedom, DOFs) close to 10^6 are widely used in common practise. The possible manner in which stringers, spar caps, spar webs, panels, ribs are introduced into FE mathematical models is part of the knowledge of structural analysts. A short discussion of this issue follows. Satsangi and Murkhopadhyay [10] used 8-node plate elements assuming the same displacement field for stiffeners and plates. Kolli and Chandrashekhara [11] formulated an FE model with 9-node plate and 3-node beam elements. Recently, Thinh and Khoa [12] have developed a new 9-node rectangular plate model to study the free vibrations of shell structures with arbitrary oriented stiffeners. It is often necessary to model stiffeners out of the plate or shell element plane. In this case beam nodes are connected to the shell element nodes via rigid fictitious links. This methodology presents some inconsistencies. The main problem is that the out-of-plane warping displacements in the stiffener section are neglected and the beam torsional rigidity is not correctly predicted. Several solutions have been proposed in the literature to overcome this issue. For instance, Vörös [13, 14] proposed a procedure to model the connection between the plate or shell and the stiffener where the shear deformation of the beam is neglected and the formulation of the stiffener is based on the well-known *Bernoulli-Vlasov* [15]

theory. In order to maintain the displacement compatibility between the beam and the stiffened element, a special transformation was used, which included torsional-bending coupling and the eccentricity of internal forces between the stiffener and the plate elements. In this chapter, a novel approach to the analysis of aircraft structures is proposed. The present CW method deals with shells and stiffeners by means of a unique one-dimensional formulation, with no need for the introduction of fictitious links to connect beam and shell elements.

As far as composite structures are concerned, many techniques are available to compute accurate stress/strain fields in the various components of a laminated structure (*i.e.* fibres, matrices and layers); these techniques are briefly discussed hereafter. The natural manner of refining the analysis of one- and two-dimensional components consists of using three-dimensional solid finite elements. These elements can be employed to discretise single components (fibres and matrices) or to directly model the layer of a laminated structure; fibres and matrices can be modeled as independent elements or they can be homogenised to compute layer properties. Because of the limitations on the aspect ratio of three-dimensional elements and the high number of layers used in real applications, computational costs of a solid model can be prohibitive. Classical theories which are known for traditional beam and plate or shell structures have been improved for application to laminates. There are many contributions based on different approaches: higher-order models [16, 17], zig-zag theories [18–21] and layer-wise (LW) approaches [22–24]. So-called *global-local* approaches have also been developed by exploiting the superposition of equivalent single layer models (ESL) and LW [25], or by using the Arlequin method to combine higher- and lower-order theories [26, 27]. Many studies on multiscale problems in composites have recently been conducted as in [28–33]; one of the most important results is that "processes that occur at a certain scale govern the behavior of the system across several (usually larger) scales" [34]. This result implies that the development of analysis capabilities involving many scale levels is necessary in order properly to understand multi-scale phenomena in composites. However, the most critical issues of many multiscale approaches proposed in literature are related to the high computational costs required (in some cases hundreds of million of degrees of freedom) and the need for material properties at nano-, micro- and macro-scale. These aspects can affect the reliability and applicability of these approaches. In this chapter, applications of the CW method to the analysis of composite structures are shown. CW models are able separately to model each typical component of a composite structure by means of a unique one-dimensional formulation. Moreover, in a given model, different scale components can be used simultaneously, that is, homogenised laminates or laminae can be interfaced with fibres and matrices. Such a model could be seen as a 'global-local' model since it can be used either to create a global model by considering the full laminate or to obtain a local model to detect accurate strain or stress distributions in those parts of the structure which could be most likely affected by failure. In other words, the present modeling approach allows us to obtain progressively refined models up to the fibre and matrix dimensions.

In the following a brief overview of CUF is provided and the CW approach is dis-

cussed. Then static and free vibration analysis of a number of structures is presented, including composite laminates, typical aircraft structures, and civil engineering buildings. The results by CW models are compared to classical beam theories, refined one-dimensional models (Taylor-expansion-based CUF models), solid and shell FE models from a commercial code, and analytical solutions when available. Finally the main conclusions are outlined.

2 Preliminaries

The adopted coordinate frame is presented in Figure 1. The beam boundaries over y are $0 \leq y \leq L$. The displacement vector is:
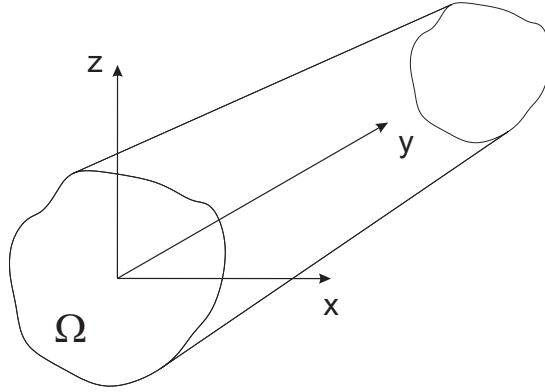

Figure 1: Coordinate frame of the beam model

$$\mathbf{u}(x, y, z) = \left\{ \begin{array}{ccc} u_x & u_y & u_z \end{array} \right\}^T \tag{1}$$

The superscript "T" represents the transposition operator. Stress, $\boldsymbol{\sigma}$, and strain, $\boldsymbol{\epsilon}$, components are grouped as follows:

$$\boldsymbol{\sigma}_p = \left\{ \begin{array}{ccc} \sigma_{zz} & \sigma_{xx} & \sigma_{zx} \end{array} \right\}^T, \quad \boldsymbol{\epsilon}_p = \left\{ \begin{array}{ccc} \epsilon_{zz} & \epsilon_{xx} & \epsilon_{zx} \end{array} \right\}^T$$
$$\boldsymbol{\sigma}_n = \left\{ \begin{array}{ccc} \sigma_{zy} & \sigma_{xy} & \sigma_{yy} \end{array} \right\}^T, \quad \boldsymbol{\epsilon}_n = \left\{ \begin{array}{ccc} \epsilon_{zy} & \epsilon_{xy} & \epsilon_{yy} \end{array} \right\}^T \tag{2}$$

The subscript "n" stands for terms lying on the cross-section, while "p" stands for terms lying on planes which are orthogonal to Ω. Linear strain-displacement relations are used:

$$\boldsymbol{\epsilon}_p = \boldsymbol{D}_p \mathbf{u}$$
$$\boldsymbol{\epsilon}_n = \boldsymbol{D}_n \mathbf{u} = (\boldsymbol{D}_{n\Omega} + \boldsymbol{D}_{ny}) \mathbf{u} \tag{3}$$

With:

$$\boldsymbol{D}_p = \begin{bmatrix} 0 & 0 & \frac{\partial}{\partial z} \\ \frac{\partial}{\partial x} & 0 & 0 \\ \frac{\partial}{\partial z} & 0 & \frac{\partial}{\partial x} \end{bmatrix}, \quad \boldsymbol{D}_{n\Omega} = \begin{bmatrix} 0 & 0 & 0 \\ 0 & \frac{\partial}{\partial x} & 0 \\ 0 & \frac{\partial}{\partial z} & 0 \end{bmatrix}, \quad \boldsymbol{D}_{ny} = \begin{bmatrix} 0 & \frac{\partial}{\partial y} & 0 \\ \frac{\partial}{\partial y} & 0 & 0 \\ 0 & 0 & \frac{\partial}{\partial y} \end{bmatrix} \tag{4}$$

The Hooke law is exploited:

$$\boldsymbol{\sigma} = \boldsymbol{C}\boldsymbol{\epsilon} \tag{5}$$

According to Equation (2), the previous equation becomes:

$$\begin{aligned}
\boldsymbol{\sigma}_p &= \tilde{\boldsymbol{C}}_{pp}\boldsymbol{\epsilon}_p + \tilde{\boldsymbol{C}}_{pn}\boldsymbol{\epsilon}_n \\
\boldsymbol{\sigma}_n &= \tilde{\boldsymbol{C}}_{np}\boldsymbol{\epsilon}_p + \tilde{\boldsymbol{C}}_{nn}\boldsymbol{\epsilon}_n
\end{aligned} \tag{6}$$

where $\tilde{\boldsymbol{C}}_{pp}$, $\tilde{\boldsymbol{C}}_{pn}$, $\tilde{\boldsymbol{C}}_{np}$, and $\tilde{\boldsymbol{C}}_{nn}$ are the material coefficient matrices whose explicit expressions are

$$\widetilde{\boldsymbol{C}}_{pp} = \begin{bmatrix} \widetilde{C}_{11} & \widetilde{C}_{12} & 0 \\ \widetilde{C}_{12} & \widetilde{C}_{22} & 0 \\ 0 & 0 & \widetilde{C}_{44} \end{bmatrix}, \quad \widetilde{\boldsymbol{C}}_{pn} = \widetilde{\boldsymbol{C}}_{np}^T = \begin{bmatrix} 0 & \widetilde{C}_{16} & \widetilde{C}_{13} \\ 0 & \widetilde{C}_{26} & \widetilde{C}_{23} \\ \widetilde{C}_{45} & 0 & 0 \end{bmatrix},$$

$$\widetilde{\boldsymbol{C}}_{nn} = \begin{bmatrix} \widetilde{C}_{55} & 0 & 0 \\ 0 & \widetilde{C}_{66} & \widetilde{C}_{36} \\ 0 & \widetilde{C}_{36} & \widetilde{C}_{33} \end{bmatrix} \tag{7}$$

Coefficients $[\tilde{C}]_{ij}$ depend on Young's and Poisson's moduli as well as on the fibre orientation angle, θ, that is graphically defined in Figure 2 where '1', '2', and '3' represent the cartesian axes of the material. For the sake of brevity, the expressions of coefficients $[\tilde{C}]_{ij}$ are not reported here, but can be found in the books by [35] or [36].
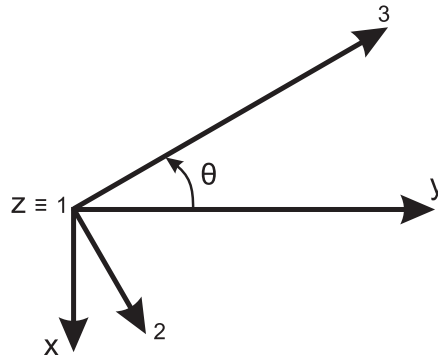

Figure 2: Fibre orientation angle

3 Unified finite element formulation

In the framework of the Carrera unified formulation (CUF), the displacement field is the expansion of generic functions, F_τ:

$$\mathbf{u} = F_\tau \mathbf{u}_\tau, \qquad \tau = 1, 2, ..., M \tag{8}$$

where F_τ vary above the cross-section. $\mathbf{u}_\tau$ is the displacement vector and M stands for the number of terms of the expansion. According to the Einstein notation, the repeated subscript, τ, indicates summation. Taylor-type expansions have been exploited in previous works by [5,37–43]. The Euler-Bernoulli (EBBT) and Timoshenko (TBT) classical theories are derived from the linear Taylor-type expansion. Lagrange polynomials are herein used to describe the cross-section displacement field. Three-, L3, four-, L4, and nine-point, L9, polynomials are adopted. L3 polynomials are defined on a triangular domain which is identified by three points. These points define the element that is used to model the displacement field above the cross-section. Similarly, L4 and L9 cross-section elements are defined on quadrilateral domains. The isoparametric formulation is exploited. In the case of the L3 element, the interpolation functions are given by [44]:

$$F_1 = 1 - r - s \qquad F_2 = r \qquad F_3 = s \qquad (9)$$

where r and s belong to the triangular domain defined by the points in Table 1.

Point	r_τ	s_τ
1	0	0
2	1	0
3	0	1

Table 1: L3 cross-section element point natural coordinates

Figure 3(a) shows the point locations in actual coordinates. The L4 element interpolation functions are given by:

$$F_\tau = \frac{1}{4}(1 + r\, r_\tau)(1 + s\, s_\tau) \qquad \tau = 1, 2, 3, 4 \qquad (10)$$

where r and s vary from -1 to $+1$. Figure 3(b) shows the point locations and Table 2 reports the point natural coordinates.

Point	r_τ	s_τ
1	-1	-1
2	1	-1
3	1	1
4	-1	1

Table 2: L4 cross-section element point natural coordinates

In the case of a L9 element the interpolation functions are given by:

$$F_\tau = \tfrac{1}{4}(r^2 + r\, r_\tau)(s^2 + s\, s_\tau) \qquad\qquad \tau = 1, 3, 5, 7$$

$$F_\tau = \tfrac{1}{2}s_\tau^2(s^2 - s\, s_\tau)(1 - r^2) + \tfrac{1}{2}r_\tau^2(r^2 - r\, r_\tau)(1 - s^2) \quad \tau = 2, 4, 6, 8 \qquad (11)$$

$$F_\tau = (1 - r^2)(1 - s^2) \qquad\qquad \tau = 9$$

(a) Three-point element, L3

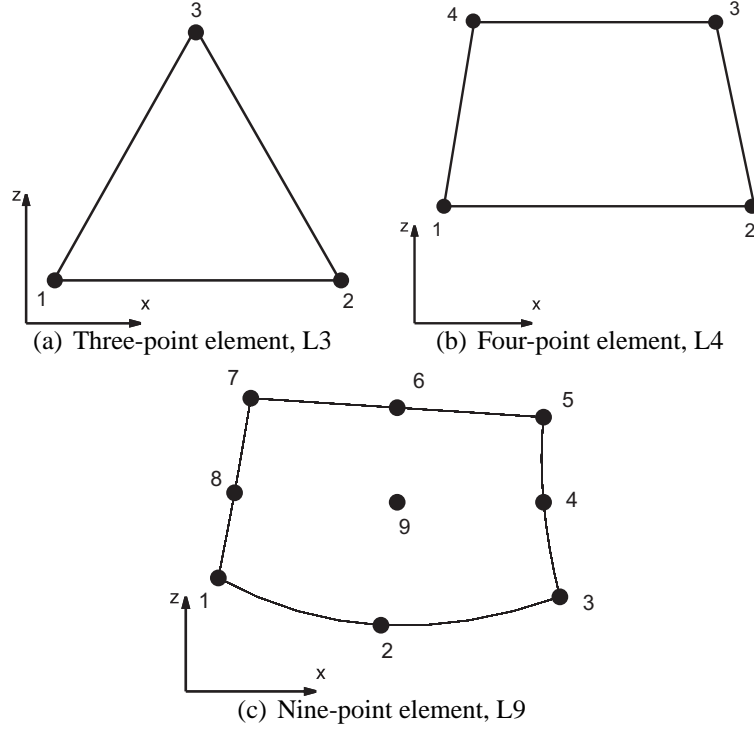(b) Four-point element, L4

(c) Nine-point element, L9

Figure 3: Cross-Section elements in actual geometry

where r and s from -1 to $+1$. Figure 3(c) shows the point locations and Table 3 reports the point natural coordinates. The displacement field given by an L4 element is:

$$
\begin{aligned}
u_x &= F_1 \, u_{x_1} + F_2 \, u_{x_2} + F_3 \, u_{x_3} + F_4 \, u_{x_4} \\
u_y &= F_1 \, u_{y_1} + F_2 \, u_{y_2} + F_3 \, u_{y_3} + F_4 \, u_{y_4} \\
u_z &= F_1 \, u_{z_1} + F_2 \, u_{z_2} + F_3 \, u_{z_3} + F_4 \, u_{z_4}
\end{aligned}
\tag{12}
$$

where $u_{x_1}, ..., u_{z_4}$ are the displacement variables of the problem and they represent the translational displacement components of each of the four points of the L4 element.

Point	r_τ	s_τ
1	-1	-1
2	0	-1
3	1	-1
4	1	0
5	1	1
6	0	1
7	-1	1
8	-1	0
9	0	0

Table 3: L9 cross-section element point natural coordinates

7

The cross-section can be discretised by means of several L-elements. Figure 4 shows the assembly of two L9 elements which share a common edge and three points.
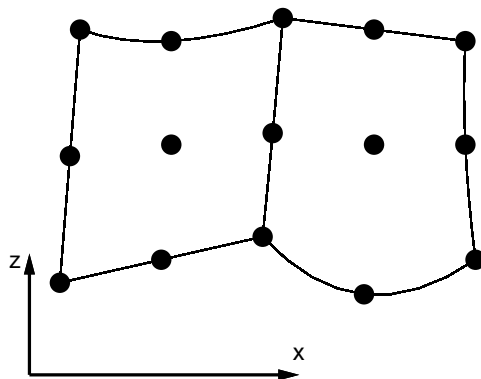

Figure 4: Two assembled L9 elements

The discretization along the beam axis is conducted via a classical finite element approach. The displacement vector is given by:

$$\mathbf{u} = N_i F_\tau \mathbf{q}_{\tau i} \tag{13}$$

where N_i stands for the shape functions and $\mathbf{q}_{\tau i}$ for the nodal displacement vector:

$$\mathbf{q}_{\tau i} = \left\{ \begin{array}{ccc} q_{u_{x_{\tau i}}} & q_{u_{y_{\tau i}}} & q_{u_{z_{\tau i}}} \end{array} \right\}^T \tag{14}$$

For the sake of brevity, the shape functions are not reported here. They can be found in many books, for instance in [45]. Elements with four nodes (B4) are herein formulated, that is, a cubic approximation along the y axis is adopted. It has to be highlighted that the adopted cross-section displacement field model defines the beam theory. It is therefore possible to deal with linear (L3), bilinear (L4), and quadratic (L9) beam theories. Further refinements can be obtained by adding cross-section elements, in this case the beam model will be defined by the number of cross-section elements used. The choice of the cross-section discretization (*i.e.* the choice of the type, the number and the distribution of cross-section elements) is completely independent of the choice of the beam finite element to be used along the beam axis. The present formulation has to be considered as an one-dimensional model since the unknowns of the problem, *i.e.* the nodal unknowns, vary along the beam axis whereas the displacement field of the beam is axiomatically modeled above the cross-section domain. The introduction of the Lagrange-like discretization above the cross-section allows us to deal with locally refinable one-dimensional models having only displacement variables.

The stiffness matrix and the mass matrix of the elements and the external loadings, which are consistent with the model, are obtained via the principle of virtual

displacements:

$$\delta L_{int} = \int_V (\delta\boldsymbol{\epsilon}_p^T \boldsymbol{\sigma}_p + \delta\boldsymbol{\epsilon}_n^T \boldsymbol{\sigma}_n) dV = \delta L_{ext} - \delta L_{ine} \qquad (15)$$

where L_{int} stands for the strain energy, and L_{ext} is the work of the external loadings, and δL_{ine} is the work of the inertial loadings. δ stands for the virtual variation. The virtual variation of the strain energy is rewritten using Equations (3), (6) and (13):

$$\delta L_{int} = \delta\mathbf{q}_{\tau i}^T \mathbf{K}^{ij\tau s} \mathbf{q}_{sj} \qquad (16)$$

where $\mathbf{K}^{ij\tau s}$ is the stiffness matrix in the form of the fundamental nucleus. In a compact notation, it can be written as:

$$
\begin{aligned}
\boldsymbol{K}^{ij\tau s} = \ & I_l^{ij} \triangleleft \left(\boldsymbol{D}_{np}^T F_\tau \boldsymbol{I}\right) \left[\tilde{\boldsymbol{C}}_{np}\left(\boldsymbol{D}_p F_s \boldsymbol{I}\right) + \tilde{\boldsymbol{C}}_{nn}\left(\boldsymbol{D}_{np} F_s \boldsymbol{I}\right)\right] + \\
& \left(\boldsymbol{D}_p^T F_\tau \boldsymbol{I}\right) \left[\tilde{\boldsymbol{C}}_{pp}\left(\boldsymbol{D}_p F_s \boldsymbol{I}\right) + \tilde{\boldsymbol{C}}_{pn}\left(\boldsymbol{D}_{np} F_s \boldsymbol{I}\right)\right] \triangleright_\Omega + \\
& I_l^{ij,y} \triangleleft \left[\left(\boldsymbol{D}_{np}^T F_\tau \boldsymbol{I}\right)\tilde{\boldsymbol{C}}_{nn} + \left(\boldsymbol{D}_p^T F_\tau \boldsymbol{I}\right)\tilde{\boldsymbol{C}}_{pn}\right] F_s \triangleright_\Omega \boldsymbol{I}_{\Omega y} + \\
& I_l^{i,y j} \boldsymbol{I}_{\Omega y} \triangleleft F_\tau \left[\tilde{\boldsymbol{C}}_{np}\left(\boldsymbol{D}_p F_s \boldsymbol{I}\right) + \tilde{\boldsymbol{C}}_{nn}\left(\boldsymbol{D}_{np} F_s \boldsymbol{I}\right)\right] \triangleright_\Omega + \\
& I_l^{i,y j,y} \boldsymbol{I}_{\Omega y} \triangleleft F_\tau \tilde{\boldsymbol{C}}_{nn} F_s \triangleright_\Omega \boldsymbol{I}_{\Omega y}
\end{aligned}
\qquad (17)
$$

where:

$$
\boldsymbol{I}_{\Omega y} = \begin{bmatrix} 0 & 1 & 0 \\ 1 & 0 & 0 \\ 0 & 0 & 1 \end{bmatrix}
\qquad \triangleleft \dots \triangleright_\Omega = \int_\Omega \dots d\Omega \qquad (18)
$$

$$
\left(I_l^{ij},\ I_l^{ij,y},\ I_l^{i,y j},\ I_l^{i,y j,y}\right) = \int_l \left(N_i N_j,\ N_i N_{j,y},\ N_{i,y} N_j,\ N_{i,y} N_{j,y}\right) dy \qquad (19)
$$

It should be noted that no assumptions on the approximation order have been made. It is therefore possible to obtain refined beam models without changing the formal expression of the nucleus components. This is the key-point of CUF which permits, with only nine FORTRAN statements, implementation of any-order beam theories. The shear locking is corrected through the selective integration (see [45]). The line and surface integral computation is numerically performed by means of the Gauss method. The assembly procedure of the Lagrange-type elements is analogous to the one followed in the case of two-dimensional elements. The procedure keypoints are briefly listed:

1. The fundamental nucleus is exploited to compute the stiffness matrix of each cross-section element of a structural node. If an L4 element is considered, this matrix will have 12×12 terms.

2. The stiffness matrix of the structural node is then assembled by considering all the cross-section elements and exploiting their connectivity.

3. The stiffness matrix of each beam element is computed and assembled in the global stiffness matrix.

The variationally coherent loadings vector is derived in the case of a generic concentrated load $\mathbf{P}$:

$$\mathbf{P} = \left\{ \begin{array}{ccc} P_{u_x} & P_{u_y} & P_{u_z} \end{array} \right\}^T \tag{20}$$

Any other loading condition can be similarly treated. The virtual work due to $\mathbf{P}$ is:

$$\delta L_{ext} = \mathbf{P}\delta\mathbf{u}^T \tag{21}$$

The virtual variation of $\mathbf{u}$ in the framework of CUF is:

$$\delta L_{ext} = F_\tau \mathbf{P}\delta\mathbf{u}_\tau^T \tag{22}$$

By introducing the nodal displacements and the shape functions, the previous equation becomes:

$$\delta L_{ext} = F_\tau N_i \mathbf{P}\delta\mathbf{q}_{\tau i}^T \tag{23}$$

This last equation permits us to identify the components of the nucleus which have to be loaded, that is, it leads to the proper assembling of the loading vector by detecting the displacement variables that have to be loaded.

The virtual variation of the work of the inertial loadings is:

$$\delta L_{ine} = \int_V \rho\delta\mathbf{u}^T \ddot{\mathbf{u}}dV \tag{24}$$

where ρ stands for the density of the material, and $\ddot{\mathbf{u}}$ is the acceleration vector. Equation (24) is rewritten using Equation (13):

$$\delta L_{ine} = \delta\mathbf{q}_{\tau i}^T \int_l N_i N_j dy \int_\Omega \rho F_\tau F_s d\Omega \ddot{\mathbf{q}}_{sj} = \delta\mathbf{q}_{\tau i}^T \mathbf{M}^{ij\tau s} \ddot{\mathbf{q}}_{sj} \tag{25}$$

where $\mathbf{M}^{ij\tau s}$ is the fundamental nucleus of the mass matrix. Its components are:

$$\mathbf{M}_{xx}^{ij\tau s} = \mathbf{M}_{yy}^{ij\tau s} = \mathbf{M}_{zz}^{ij\tau s} = \rho \int_l N_i N_j dy \int_\Omega F_\tau F_s d\Omega$$

$$\mathbf{M}_{xy}^{ij\tau s} = \mathbf{M}_{xz}^{ij\tau s} = \mathbf{M}_{yx}^{ij\tau s} = \mathbf{M}_{yz}^{ij\tau s} = \mathbf{M}_{zx}^{ij\tau s} = \mathbf{M}_{zy}^{ij\tau s} = 0 \tag{26}$$

The imposition of constraints can be carried out by considering each of the three degrees of freedom of cross-section element points independently. In other words, a constraint can be either imposed on the whole cross-section or on an arbitrary number of cross-section points.
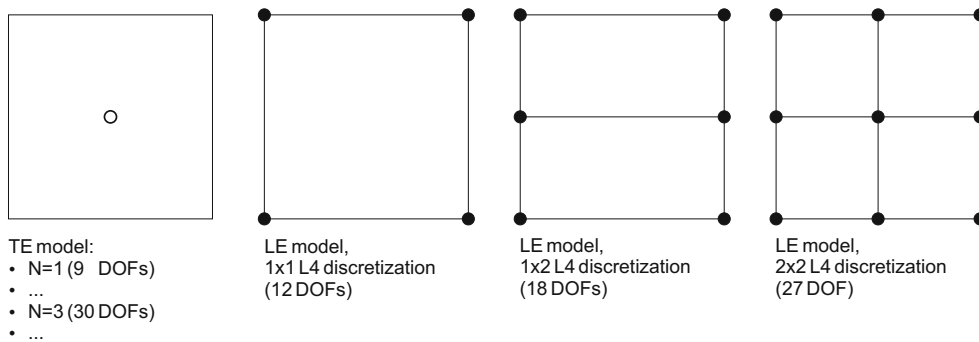
TE model:
• N=1 (9   DOFs)
• ...
• N=3 (30 DOFs)
• ...

LE model,
1x1 L4 discretization
(12 DOFs)

LE model,
1x2 L4 discretization
(18 DOFs)

LE model,
2x2 L4 discretization
(27 DOF)

Figure 5: Differences between the TE and LE models

4   The component-wise approach

The refined TE models are characterised by degrees of freedom (displacements and
N-order derivatives of displacements) with a correspondence to the axis of the beam
(see Figure 5). The expansion can also be made by using only pure displacement
values, *e.g.* by using Lagrange polynomials. The resulting LE can be used for the
whole cross-section or can be introduced by dividing the cross-section into various
sub-domains (see Figure 5). This characteristic allows us separately to model each
component of a structure. Figure 6 shows the CW approach for a four-stringer wing
box, whose components are modeled simultaneously using LE cross-sectional ele-
ments. Each component is considered with its own geometrical and material charac-
teristics. For instance, in the case of wing structures, LE expansions can adopted for
each wing section component (spars, stringer, panels), including ribs, as in Figure 6.
The resulting approach is denoted as component-wise since LE was used to identify
displacement variables in each structural component. This methodology permits us to
tune the capabilities of the model by 1. choosing which component requires a more
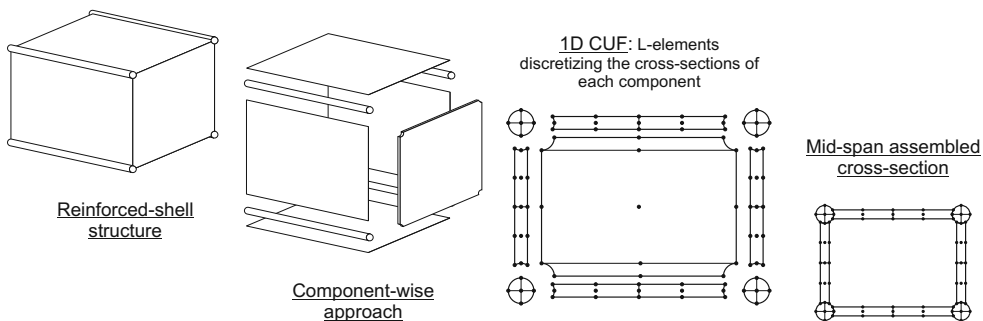detailed model; 2. setting the order of the structural model to be used.

Reinforced-shell
structure

Component-wise
approach

1D CUF: L-elements
discretizing the cross-sections of
each component

Mid-span assembled
cross-section

Figure 6: Component-wise approach to simultaneously model panels, stringers
and ribs of wing structures

11

Moreover, through the CW approach FE mathematical models can be built by only using physical surfaces; artificial lines (beam axes) and surfaces (plate or shell reference surfaces) are no longer used. This result can be obtained otherwise only using solid finite elements.

For the results provided in this chapter, LE models were implemented by means of four- (L4) and nine-point (L9) Lagrange-type polynomials over the cross-section of isotropic and composite structures, including wing reinforced-shells and civil building. To clarify the CW capabilities of the LE model, Figure 7 is proposed. Figure 7 (a) shows the cross-section of a spar composed by three stringers and two panels. The displacement field above the cross-section of each component of the spar is modeled with one nine-point Lagrange polynomial. Finally, Figure 7 (b) shows a local mode of the spar. Here, the vibration of a single component (the upper panel in this specific case) is clearly evident.

(a) Three-stringer spar modeled with L9 elements.

(b) Modal shape involving a single component.
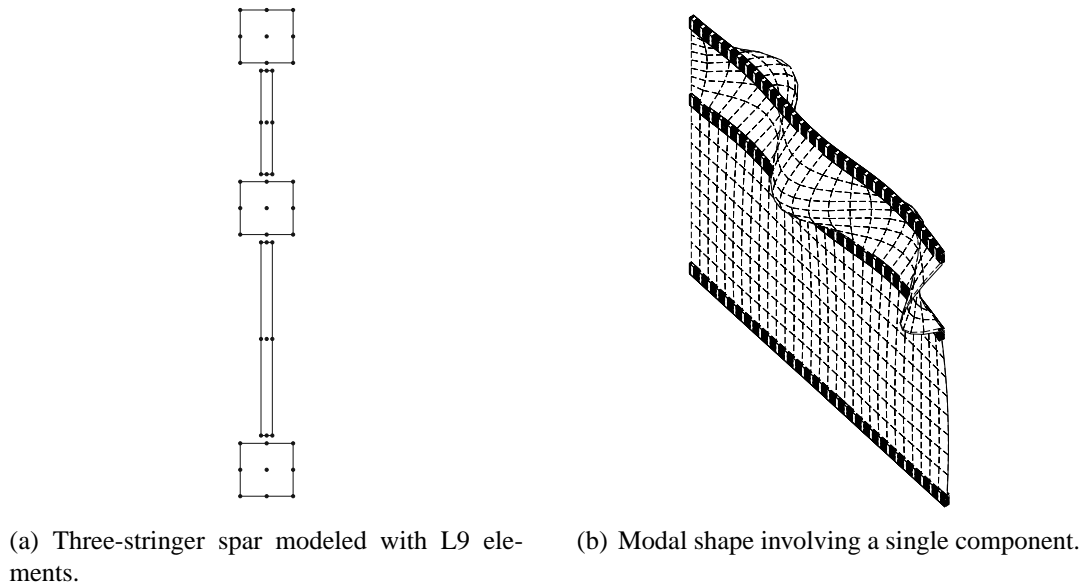
Figure 7: Component-wise capabilities of the LE models

5   Results and discussion

Several structural problems have been considered. To highlight the capabilities of Lagrange-based models, preliminary results concern problems that can be otherwise analysed only by means of solid elements. In particular, a cut hollow-square cross-section is proposed as a first assessment, then the possibility of dealing with localised constraints is shown. Afterwards, attention is given to the component-wise capabilities of the LE models. First, CW models of composite structures are proposed, including a composite spar and a cross-ply laminate. Subsequently, the application of the CW approach to the analysis of reinforced-shell wing structures is discussed. Finally, the

capabilities of the CW models in dealing with a simplified complete aircraft and civil buildings are shown. Comparisons of the results with analytical models and commercial finite element codes are provided.

5.1 Open square cross-section

An open square cross-section beam made of isotropic material was firstly considered. The material data are: the Young modulus, E, is equal to 75 [GPa]; the Poisson ratio, ν, is equal to 0.33. The cross-section geometry is shown in Figure 8.
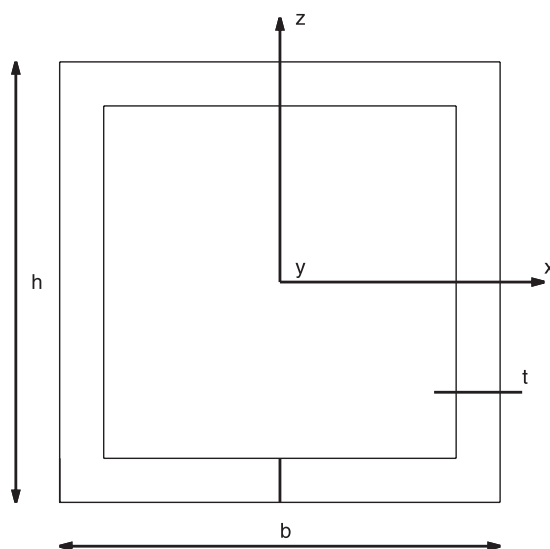

Figure 8: Open square cross-section

Both ends were clamped. The length-to-height ratio, L/h, is equal to 20. The height-to-thickness ratio, h/t, is equal to 10 with h as high as 1 $[m]$. Two opposite unit point loads, $\pm F_x$, are applied at $[0, L, -0.45]$. Three L9 distributions were adopted as shown in Figure 9.

Table 4 reports the horizontal displacement of the right-hand side loaded point which undergoes a positive horizontal force. A solid model was used to validate the results.

	DOFs	$u_x \times 10^8$ $[m]$
SOLID	131400	5.292
9 L9, Figure 20 a	5301	4.884
11 L9^a, Figure 20 b	6417	4.888
11 L9^b, Figure 20 c	6417	5.116

Table 4: Horizontal displacement, u_x, at $[0, L, -h/2]$. Open hollow square beam [6]

13

(a) 9 L9   (b) 11 L9^a (c) 11 L9^b
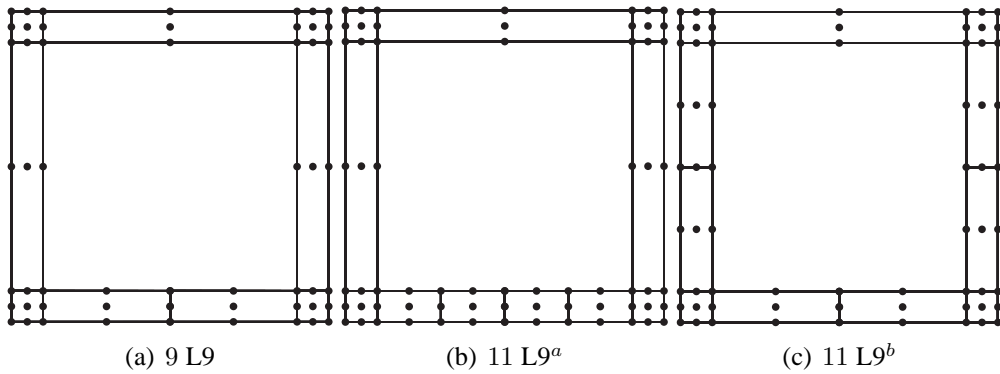
Figure 9: Cross-Section L9 distributions for the hollow square beam

The free-tip deformed cross-section is shown in Figure 10. All the considered L9 distributions together with the solid model solution are reported. Figure 11 shows the three-dimensional deformed configuration of the considered structure. The analysis of the open hollow square beam highlights the following considerations.

1. The Lagrange-based beam model is able to deal with cut cross-sections.

2. This type of problem cannot be analysed with Taylor-type beam models since the application of two opposite forces at the same point would imply null displacements.

3. The most appropriate refined L9 distribution does not necessarily lie in the proximity of load points. In this case, the most effective refinement was the one placed above the vertical braces of the cross-section which undergo severe bending deformation.

(a) 9 L9   (b) 11 L9^a (c) 11 L9^b
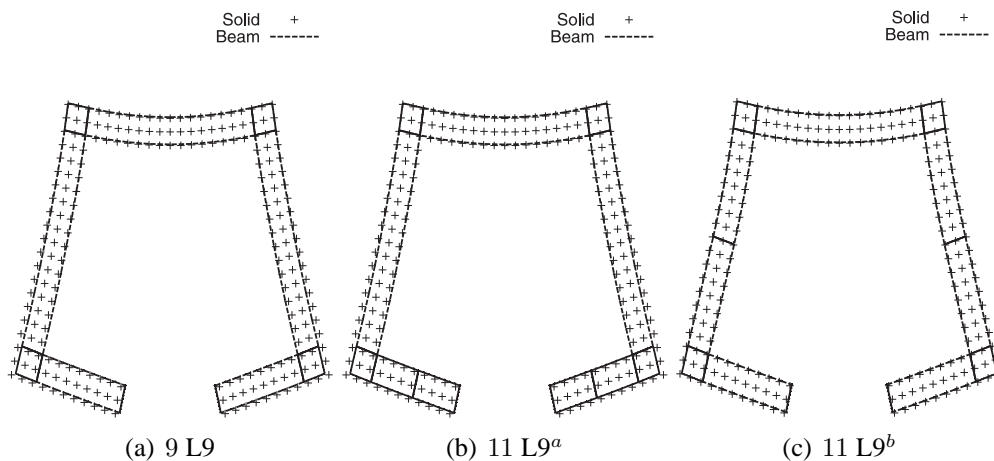
Figure 10: Deformed cross-sections of the hollow square beam [6]

14

5.2 Localised constraints over the cross-section

The present Lagrange-based beam formulation offers the important possibility of dealing with constraints that cannot be considered within classical and refined beam theories that make use of Taylor-type expansions. Beam model constraints usually act above the whole cross-section. In the framework of the present approach, each of the three degrees of freedom of every Lagrange point of the beam can be constrained independently. This means that the cross-section can be partially constrained.
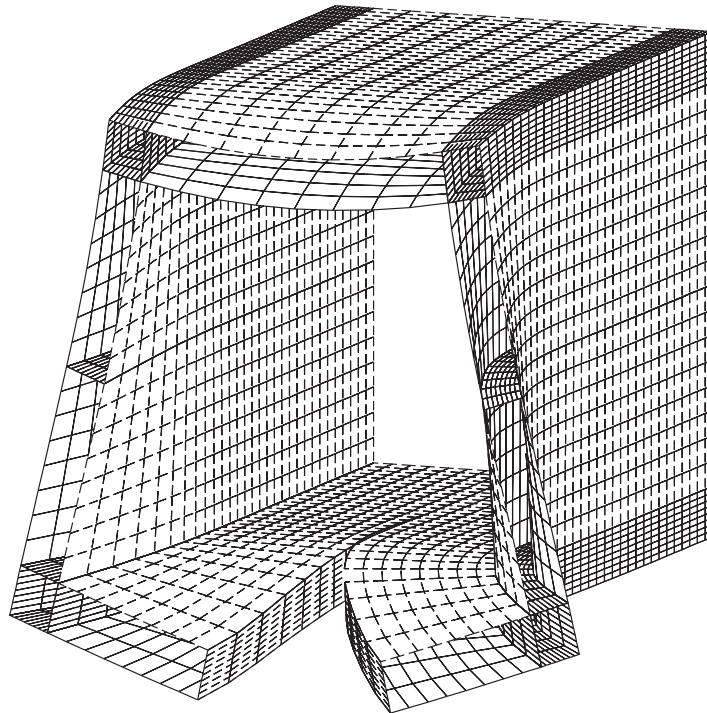
Figure 11: Three-dimensional deformed configuration of the hollow square beam. 11 L9^b [6]

A C-section beam was analysed. The structure is made of the same isotropic material as in the previous case. The cross-section geometry is shown in Figure 12. The length-to-height ratio, L/h, is equal to 20. The height-to-thickness ratio, h/t, is as high as 10 with h and b_2 equal to 1 $[m]$, and b_1 as high as $b_2/2$. Constraints were distributed along the bottom portions of the free-tip cross-sections as shown in Figure 13. Two unitary point loads, F_z, were applied at $[0, 0, 0.4]$ and $[0, L, 0.4]$, respectively. Both forces act along the negative direction. The L9 cross-section distribution is shown in Figure 15. The loaded point vertical displacement, u_z, is reported in Table 5 and compared with the value obtained from the solid model. Figures 16 and 14 show two- and three-dimensional deformed configurations, respectively.
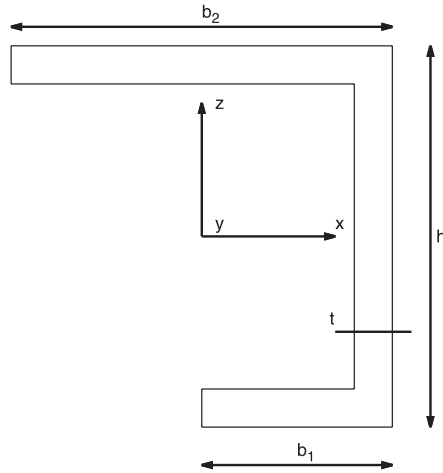
Figure 12: C-Section geometry

	DOFs	$u_z \times 10^8 \ [m]$
SOLID	84600	-3.759
13 L9[a], Figure 15	7533	-3.662

Table 5: Displacement of the loaded point of the C-section beam [6]
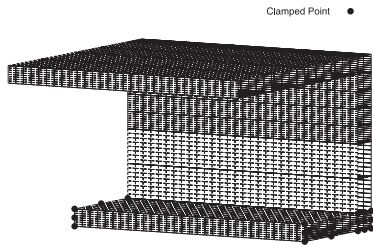

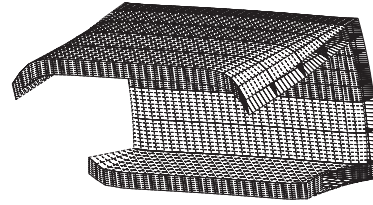Figure 13: Three-dimensional clamped point distribution on the C-section beam

Figure 14: Three-dimensional deformed configuration of the C-section beam [6]

The following conclusions can be made:

1. The results are in perfect agreement with those from solid models.

2. The proposed analysis has confirmed the possibility of dealing with partially constrained cross-section beams that is offered by the present formulation.

3. The constraints can be arbitrarily distributed in the three-dimensional directions as shown by the analysis of the C-section beam.
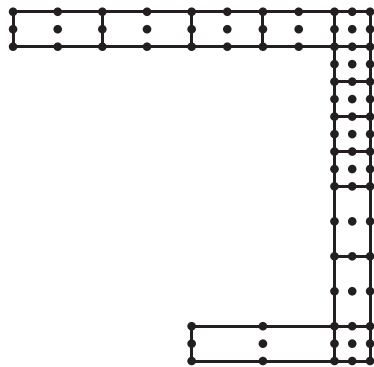
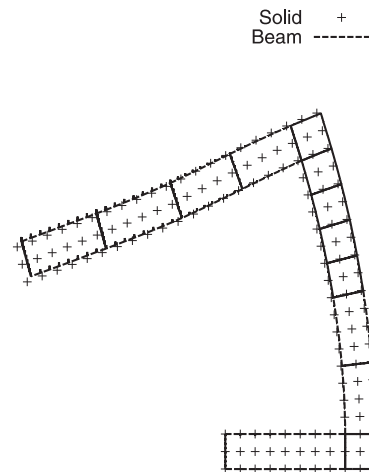Figure 15: L9 distribution above the C-section, 13 L9

Figure 16: Deformed cross-section of the C-section beam. $y = L$ [6]

5.3 Composite beams

As far as nonhomogeneous composite structures are concerned, the present component-wise approach allows us to model each typical component of a composite structure through the one-dimensional CUF formulation. Figure 17 provides a description of a possible modeling approach.
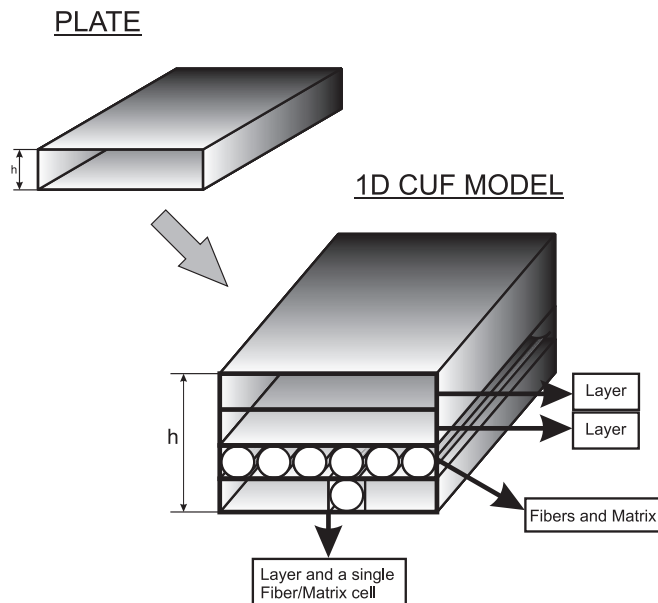

Figure 17: Component-wise approach for layers, fibres and matrices

A four-layer plate is considered and, in top-to-bottom order, the components considered are the following: the first two layers, fibres and matrix of the third layer,

the third fibre-matrix cell of the bottom layer and its remaining layer portions. Each component is considered with its own geometrical and material characteristics. A typical application of the component-wise method is based on the following analysis approach:

1. For a given composite structure, structural analysis is first conducted via classical methods (*i.e.* equivalent single layer or layer-wise).

2. The most critical zones of the structures are detected (*e.g.* those zones where stress values are critical).

3. The component-wise approach is then exploited for those critical portions in order to obtain more precise stress fields with acceptable increments of computational costs.

Figure 18 shows the matrices assembly adopted in this chapter. Independently of the choice of the components to model, both TE and LE can be used. However, using TE to obtain CW models would imply the addition of further equations imposing interface conditions. In the following, static analysis of cross-ply laminates and a composite spar is carried out.
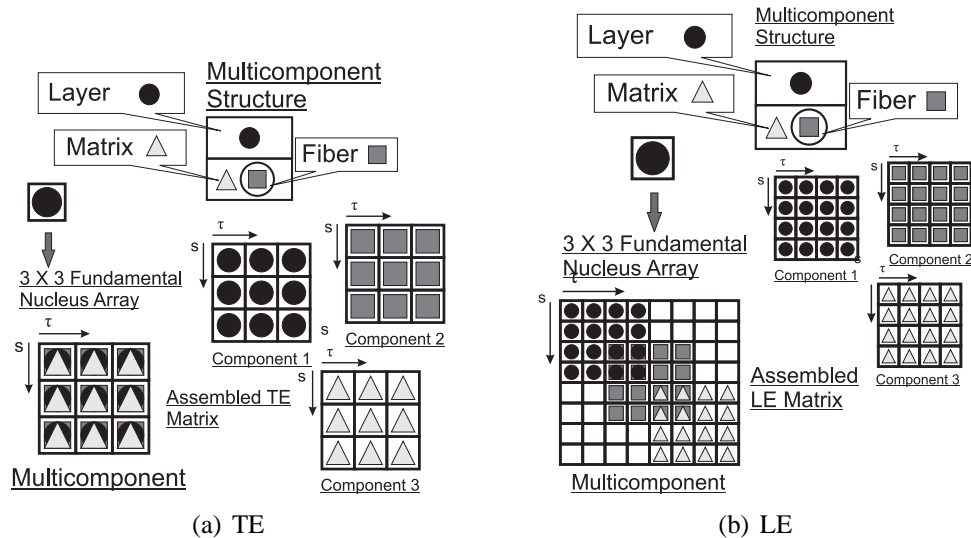

(a) TE (b) LE

Figure 18: TE and LE assembly schemes

5.3.1 Cross-ply laminate

This section deals with the structural analysis of a cantilevered laminated beam. The geometry of this model is described in Figure 19. The length of the beam, L, is $40\ [mm]$, the height (h) and the width (b) $0.6\ [mm]$ and $0.8\ [mm]$ respectively. Fibres were modeled with a circular cross-section, with a diameter, d, of $0.2\ [mm]$.
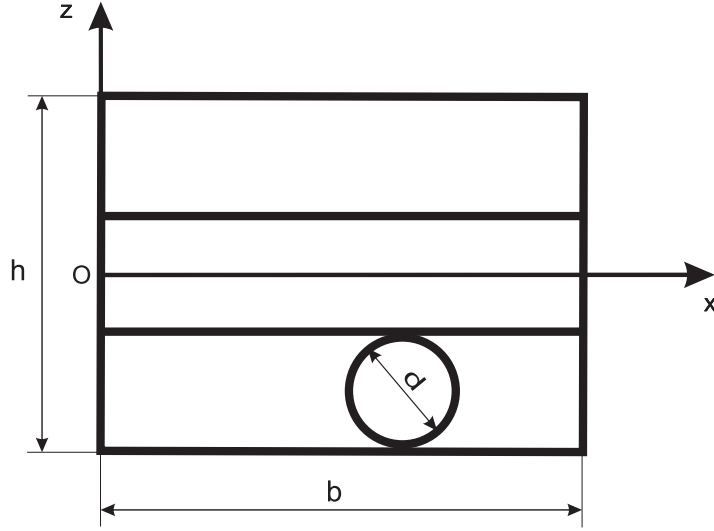
Figure 19: Geometry of the laminated plate

Four fibres per layer were considered. A point-load, F_z, was applied at $[b/2, L, 0]$, $F_z = -50\ [N]$. Fibres were considered orthotropic, with $E_L = 202.038\ [GPa]$, $E_T = E_z = 12.134\ [GPa]$, $G_{LT} = 8.358\ [GPa]$, $G_{Lz} = 8.358\ [GPa]$, $G_{Tz} = 47.756$ $[GPa]$, $\nu_{LT} = 0.2128$, $\nu_{Lz} = 0.2128$ and $\nu_{Tz} = 0.2704$. An isotropic matrix was adopted, with $E = 3.252\ [GPa]$ and $\nu = 0.355$. Layer properties were the following: $E_L = 159.380\ [GPa]$, $E_T = E_z = 14.311\ [GPa]$, $G_{LT} = 3.711\ [GPa]$, $G_{Lz} = 3.711$ $[GPa]$, $G_{Tz} = 5.209\ [GPa]$, $\nu_{LT} = 0.2433$, $\nu_{Lz} = 0.2433$ and $\nu_{Tz} = 0.2886$. Figure 20 shows the modeling approaches considered for this analysis. Both TE ($N = 4$) and LE were used for each model. In *Model 1*, the three layers of the structure were used as the components of the CW approach. In *Model 2*, the middle layer and the fibres and matrices of the top and bottom layers were considered as components. The components of *Model 3* are the top and middle layers and the bottom layer fibres and matrices. In *Model 4*, only one single fibre-matrix cell was considered.

Model	σ_{XY}^A	σ_{XY}^B
1	1.579	0.363
2	0.512	0.641
3	0.513	0.660
4	1.569	0.716

Table 6: Shear stress, $\sigma_{xy}\ [MPa]$, at two different points of the laminate, A $[0.8, 0, 0]$ and B $[0.55, 0, -0.2]$, LE models [46]

Table 7 shows the transverse displacement of the loading point and the axial stress at the center point of the third fibre of the bottom layer. This fibre is a component in *Models 2*, *3* and *4*. Shear stress values are reported in Table 6 at two different points, A (matrix) and B (fibre). Shear stress distributions above the clamped cross-section from LE models are given in Figure 21. Shear stress results are provided by means of
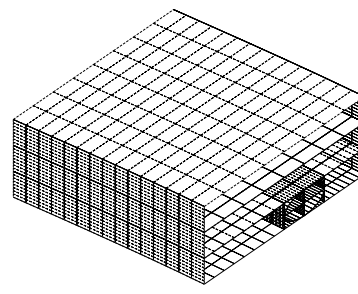
19
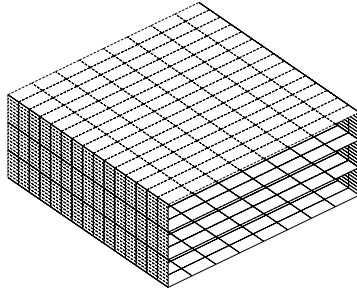
(a) *Model 1*: the three layers of the structure are the components of the CW approach
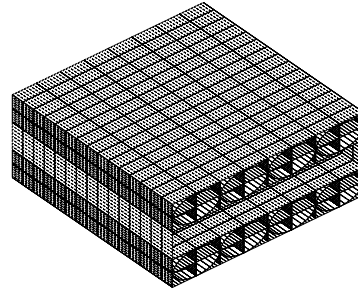
(b) *Model 2*: the middle layer and the fibres and matrices of the top and bottom layers are the components of the CW approach
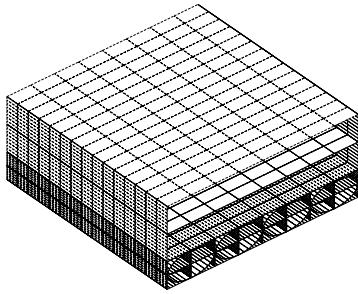
(c) *Model 3*: the top and middle layers and the fibres and matrices of the bottom layer are the components of the CW approach

(d) *Model 4*: only one fibre-matrix cell is inserted in the CW model

Figure 20: Different modeling approaches for the laminate

LE models only, because LEs give higher accuracy for shear as seen in [24].

Model	u_z [mm]	$\sigma_{yy} \times 10^{-2}$ [MPa]	DOFs
TE			
1	-9.630	-5.708	5445
2	-10.223	-7.564	5445
3	-9.921	-7.766	5445
4	-9.675	-7.295	5445
LE			
1	-9.629	-5.758	1008
2	-9.927	-7.495	7344
3	-9.775	-7.418	9024
4	-9.666	-7.264	6192

Table 7: Transverse displacement, at $[b/2, L, 0]$, and axial stress, at $[0.5, 0, -0.2]$, of the laminate [46]

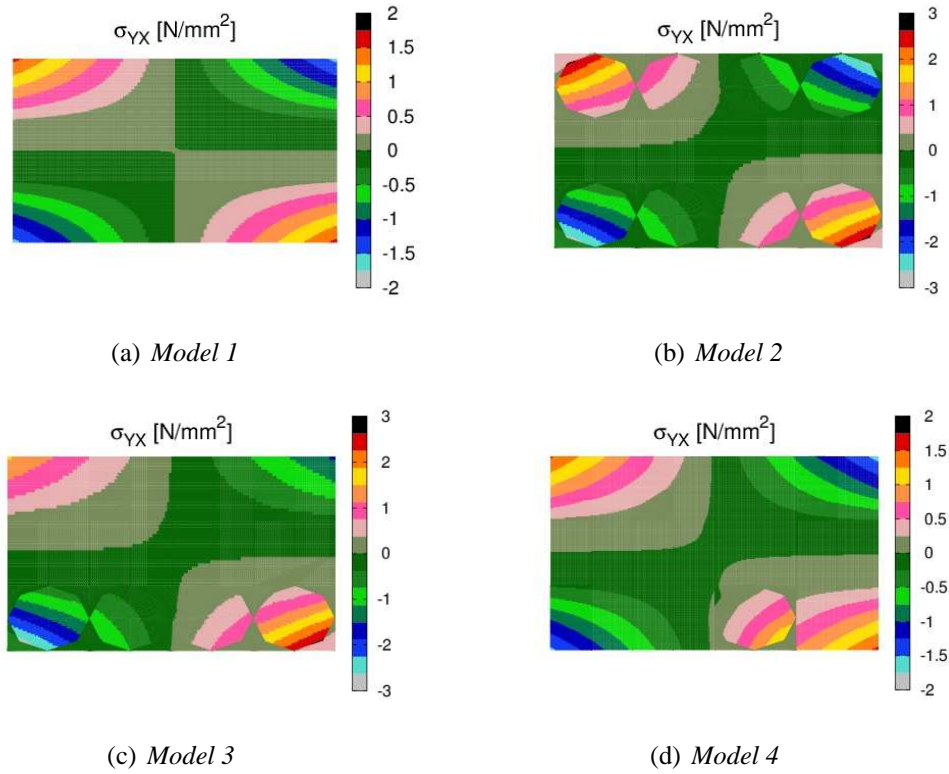The analysis of the results suggests the following:

(a) *Model 1*

(b) *Model 2*

(c) *Model 3*

(d) *Model 4*

Figure 21: Shear stress, σ_{yx}, distribution above the cross-section at $y = 0$, laminated beam, LE models [46]

1. Stress fields are significantly affected by the choice of modeling approach. Very different stress fields were detected depending on the choice of the components. This was due to the fact that homogenised material characteristics were used for layers whereas the characteristics of each component were adopted for fibres and matrices.

2. The adoption of localised fibre-matrix components (restricted to a lamina in Model 3 or to a fibre-matrix cell in Model 4) allows us to use simpler models without considerably affecting the accuracy of the result if compared to more cumbersome models. This means that if an accurate stress field is needed around a given fibre, the use of fibre-matrix components can be limited to the fibre location.

3. Displacement values are less influenced than stress fields by the choice of the modeling approach.

5.3.2 Composite-type longeron

A beam made of composite materials, assembled with different parts, was considered with the aim of analysing a typical simplified longeron structure for aerospace appli-

cations. The cross-section geometry is shown in Figure 22, where several components can be distinguished:
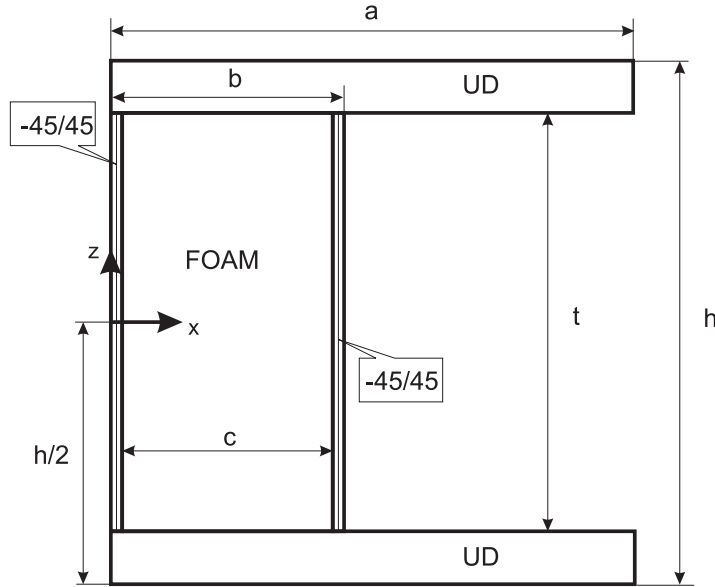

Figure 22: Composite longeron beam cross-section

1. the horizontal unidirectional, UD, top and bottom parts;

2. the foam made core;

3. the $-45/45$ vertical thin layers which coat the foam.

Table 8 shows the dimensions of the cross-section.

	$[m]$
a	0.100
b	0.044
c	0.040
h	0.100
t	0.080

Table 8: Composite longeron cross-section dimensions

The length, L, of the beam is equal to $1\,[m]$. The UD and the thin layers were made of orthotropic material, which has the following characteristics: the Young modulus along the longitudinal, E_L, is equal to $40\,[GPa]$, and those along the transverse directions are equal to $4\,[GPa]$. The Poisson ratio, ν, is equal to 0.25, and the shear modulus, G, is equal to $1\,[GPa]$; the same Poisson and shear modulus values are used in all directions. The foam core was modeled with an isotropic material with

E equal to 50 $[MPa]$, and ν equal to 0.25. It should be noted that the LE one-dimensional formulation permits us to obtain a quite convenient description of the cross-section subdomain; the adopted L9 distribution is shown in Figure 23. A unitary point load was applied to the bottom surface at $[b/2, L, -h/2]$ along the z-direction. An MSC/NASTRAN® solid model was used for comparison purposes.

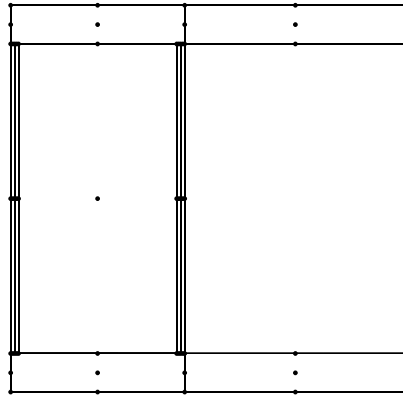

Figure 23: Cross-Section L9 distribution of the composite longeron, $9\times$ L9

Table 9 presents the vertical displacements of the loaded point obtained from using the different models. The vertical displacement distribution above the cross-section is given in Figure 24. The axial stress at $[b/2, 0, -h/2]$ is presented in Table 10. The following considerations can be made.

1. The detection of the correct displacement field as well as of the axial stress requires the present LE model, since the Taylor one presents a slow convergence for increasing theory orders.

2. Classical models foresee constant displacement distributions above the cross-section.

3. The Lagrange model is able to detect the three-dimensional solution, that is, the three-dimensional solution is detected by means of the present one-dimensional formulation.

4. The computational cost of the present one-dimensional model is much lower than that of the solid model.

5.4   Reinforced-shell wing structures

Primary aircraft structures are essentially reinforced thin shells [7]. These are so-called *semimonocoque* constructions which are obtained by assembling three main components: skins (or panels), longitudinal stiffening members (including spar caps)

	$u_z \times 10^{-6}\ [m]$	DOFs
Classical Beam Theories		
EBBT	-2.040	138
TBT	-2.224	230
TE		
$N = 1$	-2.246	414
$N = 2$	-2.286	828
$N = 3$	-2.376	1380
$N = 4$	-2.463	2070
LE		
9 L9, Figure 23	-2.800	7866
MSC/NASTRAN®		
SOLID	-2.801	250000

Table 9: Loading point vertical displacement, u_z, for the longeron model [24]

(a) TBT
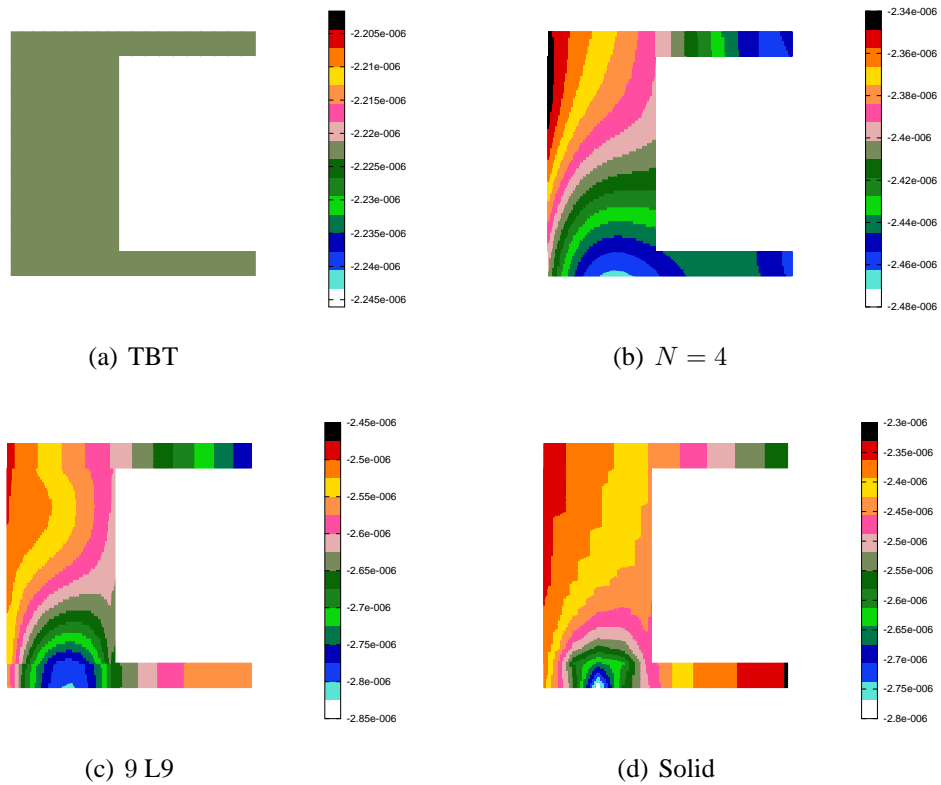
(b) $N = 4$

(c) 9 L9

(d) Solid

Figure 24: u_z-distribution above the free-tip cross-section of the composite longeron via different one-dimensional models and solids [24]

and transversal stiffeners (ribs). The determination of stress or strain fields in these structural components is of prime interest to structural analysts.

	$\sigma_{yy} \times 10^4 \ [Pa]$	DOFs
Classical Beam Theories		
EBBT	-0.113	138
TBT	-0.113	230
TE		
$N = 1$	-0.141	414
$N = 2$	-0.736	828
$N = 3$	-0.784	1380
$N = 4$	-0.813	2070
LE		
9 L9, Figure 23	-1.625	7866
MSC/NASTRAN®		
SOLID	-1.776	250000

Table 10: Axial stress, σ_{yy}, at $[c/2, 0, -h/2]$ for the longeron model [24]

The static analysis of a simple spar is considered in the following. TE and LE models are compared both with classical beam theories and solid elements of a commercial code. Analytical results based on the simplifying assumptions of the semimonocoque assembled components are provided. According to [7, 9] the internal loads in a statically determinate reinforced-shell structure can be found by the use of static equilibrium equations alone. In a statically indeterminate structure, additional equations along with the static equilibrium equations are necessary to find all the internal stresses. We should impose compatibility conditions by means of the principle of virtual displacements. This approach is hereafter referred to as the PS (pure semimonocoque) model. If EBBT is applied to the idealised semimonocoque assumptions it is possible to reduce redundancy in statically indeterminate structures. This method is hereafter referred to as BS (beam semimonocoque) model.

As far as free vibration analysis is considered, a three-stringer spar and a complete aircraft wing are addressed. The attention is focused on the capability of CW models to detect both local (component-wise) and global modal shapes.

5.4.1 Two-stringer spar

The simple spar structure shown in Figure 25 was considered. Stringers were taken to be rectangular for convenience, however their shape does not affect the validity of the proposed analysis. The geometrical data are as follows: axial length, $L = 3$ $[m]$; cross-section height, $h = 1$ $[m]$; area of the spar caps, $A_s = 0.9 \times 10^{-3}$ $[m^2]$; web thickness, $t = 1 \times 10^{-3}$ $[m]$. The whole structure is made of an aluminum alloy material. The material data are: the Young modulus, $E = 75$ $[GPa]$; Poisson ratio, $\nu = 0.33$. The beam was clamped at $y = 0$ and a point load, $F_z = -1 \times 10^4$ $[N]$, was applied at $[0, L, 0]$.

The vertical displacement, u_z, at the loaded point is reported in Table 11. Compo-
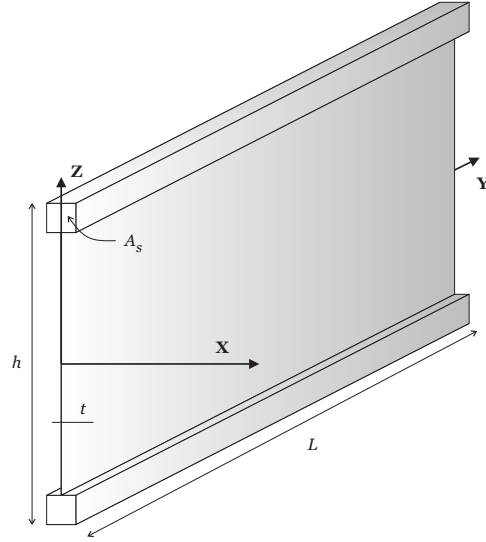
Figure 25: Two-stringer spar

	$u_z \times 10^3 \ [m]$	$P \times 10^{-4} \ [N]$	$q \times 10^{-4} \ [N/m]$	DOFs
MSC/NASTRAN®				
SOLID	-3.815	2.617	-1.036	76050
Analytical Methods				
BS	-2.671	3.192	-1.064	-
PS	-3.059	3.192	-1.064	-
Classical Beam Theories				
EBBT	-1.827	1.993	-0.274	93
TBT	-2.117	1.993	-0.274	155
TE				
$N = 3$	-2.514	2.434	-0.665	930
$N = 5$	-2.629	2.350	-0.561	1953
CW				
4 L9, Figure 26a	-3.639	3.171	-1.034	2883
8 L9, Figure 26b	-3.639	3.167	-1.035	4743

Table 11: Displacement values, u_z, at the loaded point, axial load in the upper stringer, P, at $y = 0$ and mean shear flow on the sheet panel, q, at $y = \dfrac{L}{2}$, two-stringer spar [47]

nent-wise LE results are given in last two rows. These models were obtained by using two different L9 cross-section distributions, as shown in Figure 26.

The third column in Table 11 quotes the number of the degrees of freedom for each model. The analytical results related to BS and PS approaches are evaluated as
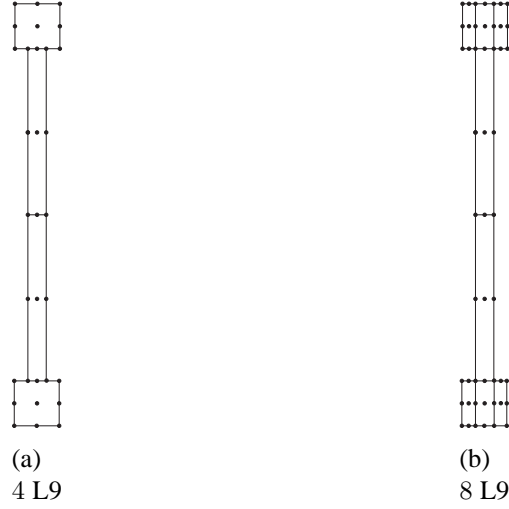
(a)
4 L9

(b)
8 L9

Figure 26: Cross-section L9 distributions for the LE models of the two-stringer spar

follows:

$$u_{z_{BS}} = \frac{F_z L^3}{3EI}, \qquad u_{z_{PS}} = \frac{F_z L^3}{3EI} + \frac{F_z L}{AG} \qquad (27)$$

where I is the cross-section moment of inertia about the x-axis, G is the shear modulus and A is the overall cross-section area. For this numerical example, stress fields are evaluated in terms of axial loads in stringers and shear flows on webs, in order to compare the results with classical analytical models. Table 11 reports the axial load in the upper stringer, P, at $y = 0$ and the mean shear flow in the panel, q, at $y = \dfrac{L}{2}$. In accordance with [9], for both BS and PS analytical models, P and q were evaluated as

$$P = \frac{F_z L}{\overline{h}}, \qquad q = -\frac{F_z}{\overline{h}} \qquad (28)$$

where $\overline{h}$ is the distance between the centers of the two stringers.

The variation in the axial stress and the shear stress versus the z-axis is presented in Figures 27. The following considerations arise from the analyses.

1. Refined beam theories, especially LE, allows us to obtain the results of the solid model (which is the most accurate and at the same time the most computationally expensive).

2. The number of degrees of freedom of the present models is significantly reduced with respect to the MSC/NASTRAN® solid model.

3. Both MSC/NASTRAN® and higher-order CUF models, unlike analytical theories based on idealised stiffened-shell structures and classical one-dimensional models, highlight the fact that the axial stress component, σ_{yy} is not linear versus z and that the shear stress component, σ_{yz}, is not constant along the sheet panel.

27
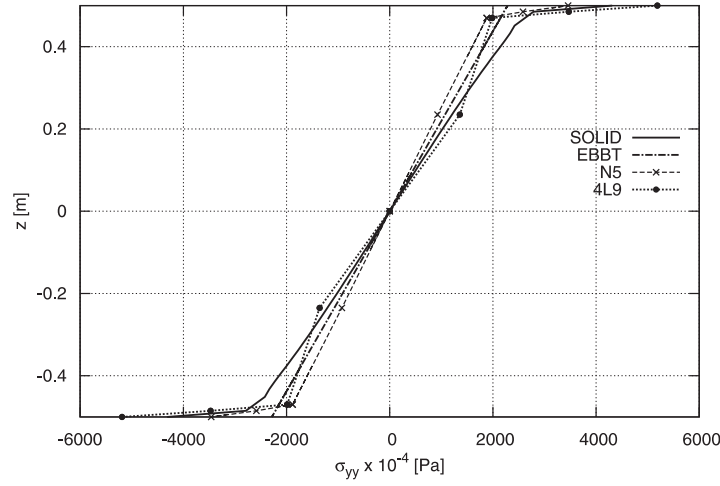
(a) σ_{yy} vs. z at $x = y = 0$
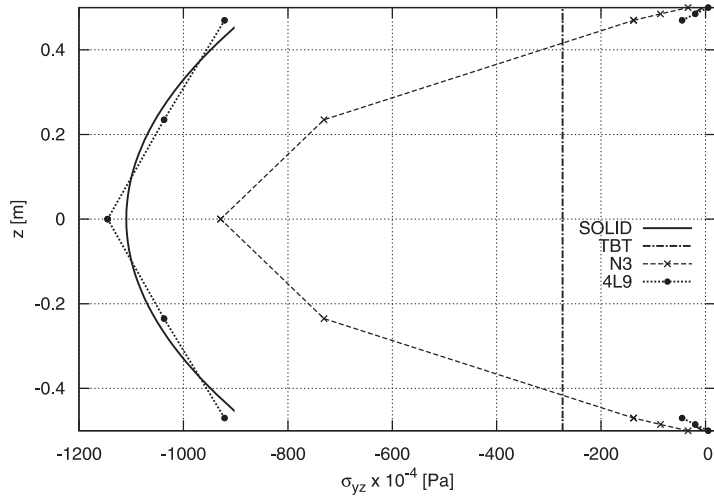
(b) σ_{yz} vs. z at $x = 0$, $y = \frac{L}{2}$

Figure 27: Axial stress, σ_{yy}, and shear stress, σ_{yz}, versus the z-axis, two-stringer spar [47]

5.4.2 Three-stringer spar

The free vibration analysis of a longeron with three longitudinal stiffeners was carried out. The geometry of the structure is shown in Figure 28.

The spar is clamped at $y = 0$. The geometrical characteristics are the following: axial length, $L = 3\ [m]$; cross-sectional height, $h = 1\ [m]$; area of the stringers , $A_s = 1.6 \times 10^{-3}\ [m^2]$; panels' thickness, $t = 2 \times 10^{-3}\ [m]$; distance between the intermediate stringer and the x-y plane, $b = 0.18\ [m]$. The whole structure is made of the same isotropic material as in the previous case.

The first fifteen natural frequencies are reported in Table 12, together with the number of the degrees of freedom for each model. The component-wise LE model was
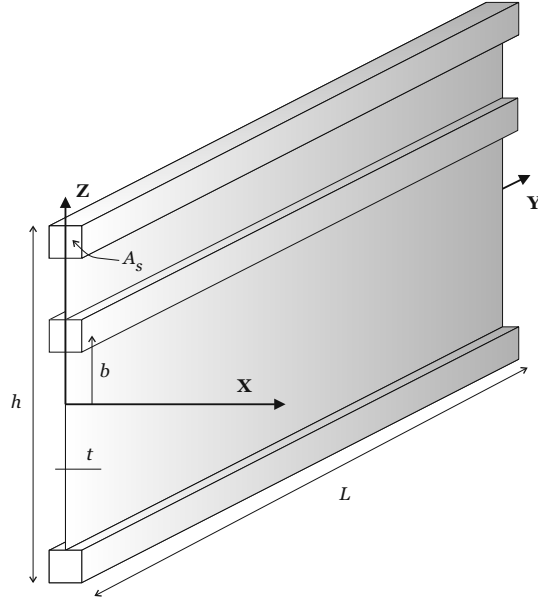
Figure 28: Three-stringer spar

	EBBT	TBT	$N=1$	$N=2$	$N=3$	$N=4$	5 L9	SOLID
DOFs	93	155	279	558	930	1395	3813	62580
Mode 1	3.24^b	3.24^b	3.24^b	3.43^b	3.35^b	3.31^b	3.46^t	3.15^b
Mode 2	20.29^b	20.28^b	20.28^b	16.70^t	16.34^t	16.13^t	3.52^b	3.55^t
Mode 3	56.81^b	56.74^b	56.74^b	21.39^b	20.97^b	20.75^b	3.76^b	3.82^b
Mode 4	111.36^b	108.81^b	108.81^b	55.25^t	52.90^t	51.70^t	14.27^s	13.30^s
Mode 5	117.60^b	111.11^b	111.11^b	60.11^b	59.23^b	58.24^b	16.73^s	15.06^s
Mode 6	184.30^b	183.57^b	183.57^b	108.19^t	100.81^t	97.87^t	17.67^s	16.33^s
Mode 7	275.94^b	274.23^b	269.29^t	109.44^b	105.55^b	102.26^b	21.17^s	19.81^s
Mode 8	386.89^b	383.36^b	274.23^b	117.79^b	116.61^b	113.20^b	21.71^t	21.49^t
Mode 9	439.21^e	439.20^e	383.36^b	181.03^t	165.23^t	119.39^s	22.95^b	22.81^b
Mode 10	517.91^b	455.17^b	439.20^e	194.59^b	183.16^s	161.07^t	25.11^s	24.07^s
Mode 11	622.84^b	511.36^b	455.17^b	276.03^t	197.98^b	176.65^s	25.73^s	24.63^s
Mode 12	669.05^b	658.20^b	511.36^b	290.25^b	229.97^s	189.01^b	31.21^s	29.69^s
Mode 13	830.95^b	817.28^b	658.20^b	325.69^s	248.76^t	243.58^t	37.92^s	36.24^s
Mode 14	1104.56^b	972.68^b	807.88^t	393.92^t	290.54^b	258.64^s	45.79^s	43.88^s
Mode 15	1317.62^e	1055.78^b	817.28^b	406.78^b	302.06^s	281.59^b	54.86^s	51.64^s

(*) b: bending mode; t: torsional mode; s: shell-like mode; e: extensional mode.

Table 12: First 15 natural frequencies $[Hz]$ of the three-stringer spar [48]

obtained by discretising the cross-section with five L9 elements, one for each spar component (stringers and webs)

The consistent correspondence between the CW model and the SOLID model was further investigated by means of the modal assurance criterion (MAC), whose graphic representation is shown in Figure 29. The MAC is defined as a scalar constant relating the degree of consistency (linearity) between one modal and another reference modal

vector [49]. MAC takes on values from zero (representing no consistent correspondence), to one (representing a consistent correspondence).
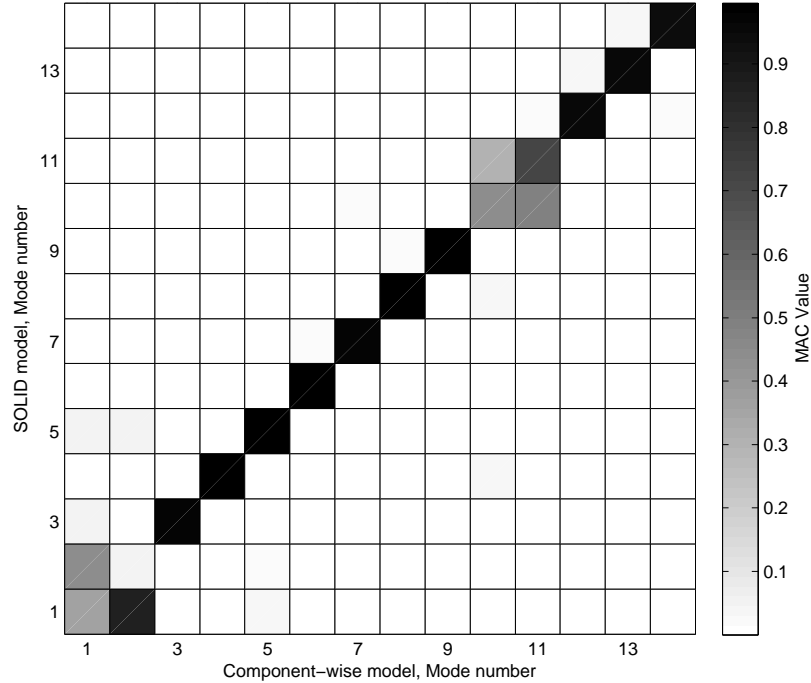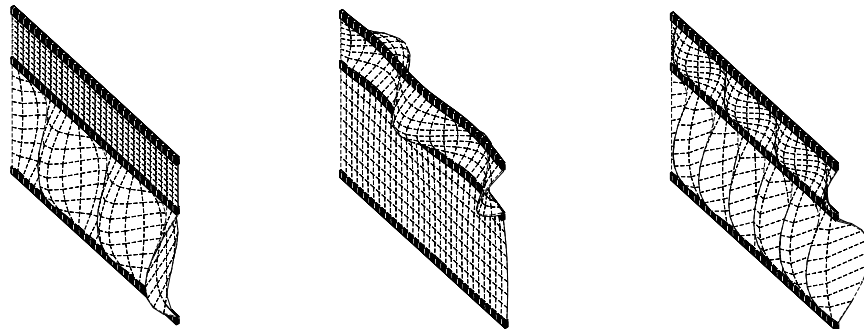

Figure 29: MAC values, three-stringer spar [48]

Up to the 14th mode there is a good correspondence between the two models. Further refinements of the LE model (*i.e.* adopting more L-elements to discretise the cross-section of the longeron) should improve this correspondence. Figure 30 shows some local modes computed with the CW model.

(a) Mode 12, $f_{12} = 31.21\ Hz$ (b) Mode 21, $f_{21} = 84.66\ Hz$ (c) Mode 29, $f_{29} = 104.99\ Hz$

Figure 30: Local modes, five L9 (LE) model of the three-stringer spar [48]

The following statements hold:

1. The classical beam theories and the linear ($N = 1$) TE model correctly detect bending and extensional modes. No torsional mode are detected.

2. To detect the torsional and shell-like modes a higher than first-order TE model is necessary. However, very high expansion orders are needed to correctly predict the frequencies of these modal shapes.

3. The CW model matches the solid FE solution with a significant reduction of the computational costs. It should be noted that the component-wise models can find typically shell-like modal shapes by means of the one-dimensional CUF.

5.4.3 Complete aircraft wing

The modal analysis of a complete aircraft wing is proposed. The cross-section of the wing is shown in Figure 31.
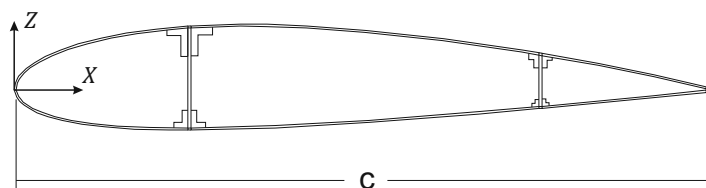

Figure 31: Cross-section of the wing

The NACA 2415 airfoil was used and two spar webs and four spar caps were added. The airfoil has the chord, c, as equal as 1 $[m]$. The length, L, along the span direction is equal to 6 $[m]$. The thickness of the panels is 3×10^{-3} $[m]$, whereas the thickness of the spar webs is 5×10^{-3} $[m]$. The whole structure is made of the same isotropic material as in the previous cases. The wing was clamped at the root. For the present wing structure, two different configurations were considered. Let *Configuration A* be the wing with no transverse stiffening members. In *Configuration B* the wing is divided into three equal bays, each separated by a rib with a thickness of 6×10^{-3} $[m]$.

Table 13 shows the main modal frequencies of both the wing's structural configurations. In this table, the results obtained through the CUF models are compared to those from classical beam theories and to those from SOLID models. In the last two rows of Table 13, the frequencies of the first two shell-like modes are quoted. The following considerations hold.

1. The bending modes of the wing are correctly detected by both the lower-order and higher-order TE models.

	EBBT	TBT	$N=1$	$N=2$	$N=3$	CW	SOLID
Configuration A							
DOFs	93	155	279	558	930	21312	186921
Global Modes							
I Bending^{x*}	4.22	4.22	4.22	4.29	4.26	4.23	4.21
I Bending^z	22.10	21.82	21.82	21.95	21.87	21.76	21.69
II Bending^x	26.44	26.36	26.36	26.66	26.25	25.15	24.78
I Torsional	-	-	132.93	50.27	48.46	31.14	29.18
III Bending^x	73.91	73.35	73.35	73.99	71.64	59.26	56.12
II Bending^z	134.66	124.68	124.68	124.99	122.77	118.39	118.00
Local Modes							
I Shell-like	-	-	-	-	-	86.36	75.13
II Shell-like	-	-	-	-	-	88.94	73.85
Configuration B							
DOFs	84	140	252	504	840	23976	171321
Global Modes							
I Bending^{x*}	4.12	4.12	4.12	4.19	4.17	4.14	4.12
I Bending^z	21.56	21.30	21.30	21.50	21.42	21.28	21.22
II Bending^x	25.71	25.63	25.63	26.00	25.61	25.00	24.92
I Torsional	-	-	131.24	49.57	47.48	39.45	39.22
III Bending^x	71.44	70.90	70.90	71.80	69.49	64.84	63.88
II Bending^z	131.11	121.49	121.49	122.23	120.06	115.76	115.40
Local Modes							
I Shell-like	-	-	-	-	-	85.61	75.01
II Shell-like	-	-	-	-	-	91.54	78.61

* Bending$^\xi$: bending mode along the ξ-axis

Table 13: Global and local modal frequencies of the complete aircraft wing [48]

2. As revealed by the previous numerical examples, at least a cubic expansion on the displacement field (TE $N=3$) is necessary to correctly detect the torsional modes.

3. The CW LE models match the SOLID solutions: shell-like modes can be obtained by means of beam elements.

4. The computational effort of a higher-order beam model is significantly lower than the ones requested by solid models.

To deal with complex structures, such as the one considered in this section, the CW models were included into a commercial software and the post-processing of the CW model of the wing has been performed with MSC/PATRAN®. Two shell-like modes evaluated by means of the CW model are shown in Figure 32 for the *Configuration A*.
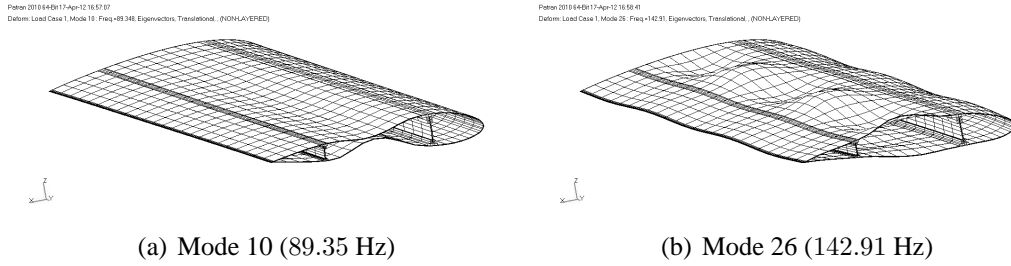
<table>
<tr><td>(a) Mode 10 (89.35 Hz)</td><td>(b) Mode 26 (142.91 Hz)</td></tr>
</table>

Figure 32: Shell-like modes of the wing (*Configuration A*) evaluated with the CW model [48]

5.5 Dynamic response of a simplified aircraft model

The dynamic response of a simplified model of aircraft was considered in order to investigate the capabilities of the present model in such an analysis. The geometry of the structure is shown in Figure 33. The geometrical shape is a function of the parameter a, which is considered as equal as $0.5\ [m]$. The structure has a constant thickness of $0.2 \times a$. The material considered is aluminium. Non constraints were considered so the structure was free.
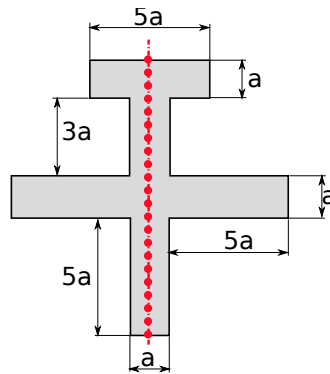

Figure 33: Geometry and beam axis of the TE model

Results from both TE and LE models are provided. In the TE model of the aircraft, a singular non-uniform cross-section beam is considered as shown in Figure 33. The CW model is obtain exploiting multiple beam elements, each discretised with an L9 cross-sectional Lagrange-element as shown in Figure 34. The first ten natural frequencies for fourth- and fifth-order TE models are reported in the first two columns of Table 14. A comparison with respect to the results from the commercial code MSC/NASTRAN® obtained using two-dimensional elements is given in the third column. The results by the CW model are quoted in column four. In Figure 35 the first eight natural modes evaluated by means of the CW model are shown. The results show that the analysis of a whole aircraft structure may be carried out by means of higher order one-dimensional models.
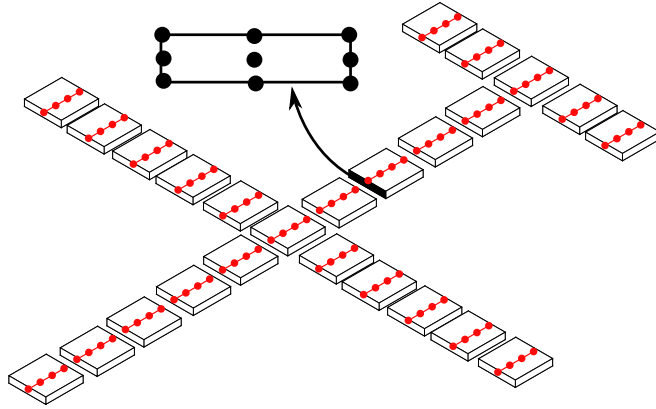
33

Figure 34: CW model of the aircraft exploiting multiple beam elements

	TE4	TE5	SHELL	LE
DOFs	2880	4032	6120	1845
1st	11.427	11.342	10.804	10.944
2nd	20.824	19.499	17.264	18.201
3rd	21.591	21.404	20.053	20.208
4th	51.448	51.137	50.372	50.398
5th	73.244	52.989	51.162	52.122
6th	62.246	59.476	51.307	52.389
7th	81.915	74.980	65.552	66.962
8th	74.791	74.612	69.942	70.633
9th	102.908	101.304	75.774	77.844
10th	88.310	87.790	87.436	89.572

Table 14: First ten natural frequencies $[Hz]$ of the simplified aircraft model [50]

(a) Mode 1   (b) Mode 2   (c) Mode 3   (d) Mode 4

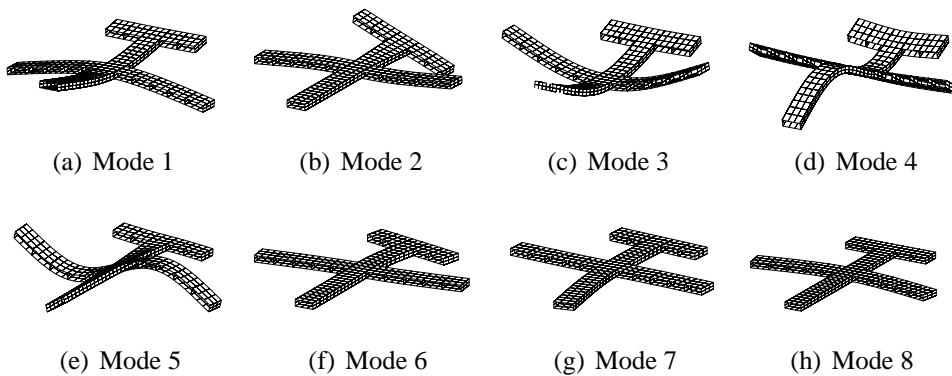(e) Mode 5   (f) Mode 6   (g) Mode 7   (h) Mode 8

Figure 35: First eight modes of the aircraft evaluated by means of the LE model [50]

5.6 Civil engineering structures

Results from the free vibration analysis of civil structures through CW models are provided here. Two structural configurations were considered, as shown in Figure 36. *Configuration A* is a one-level structure composed by four square columns made of isotropic steel material (elastic modulus $E = 210 \ [GPa]$, density $\rho = 7.5 \times 10^3 \ [Kg/m^3]$, Poisson ratio 0.28) and a floor whit properties as shown in Figure 37. The floor is made of a material whose properties are $1/5$ of those of the considered steel alloy. *Configuration B* is a three-level construction with four columns and three floors.

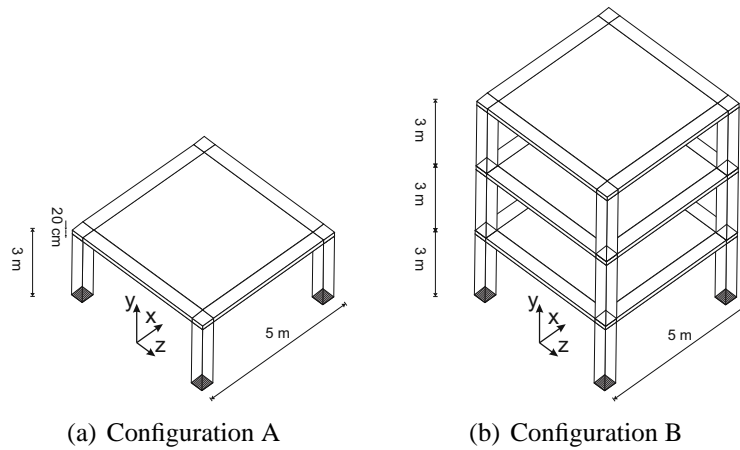

(a) Configuration A   (b) Configuration B
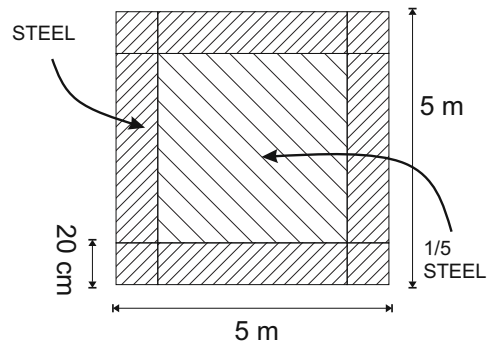
Figure 36: Civil structures

Figure 37: Floor

The CW models were obtained with a combination of L9 elements above the cross-sections. Results by CW analysis were compared to those from solid analysis by MSC/NASTRAN®. Table 15 quotes the natural frequencies together with the number of the degrees of freedom for both LE and solid models. Figure 38 shows some modal shapes of the considered civil structures evaluated through the CW models.

	Configuration A		Configuration B	
	CW	SOLID	CW	SOLID
DOFs	3396	181875	6300	78975
Mode 1	9.43^b	8.79^b	3.63^b	3.07^b
Mode 2	9.43^b	8.79^b	3.63^b	3.07^b
Mode 3	13.86^t	12.44^t	5.32^t	4.22^t
Mode 4	23.07^f	21.67^f	10.64^b	9.69^b
Mode 5	36.80^f	36.66^f	10.64^b	9.69^b
Mode 6	36.80^f	36.66^f	15.60^t	13.36^t
Mode 7	40.59^f	37.59^f	16.45^b	16.42^b
Mode 8	72.41^f	77.07^f	16.45^b	16.42^b

* b: bending mode; t: torsional mode; f: floor mode

Table 15: Natural frequencies $[Hz]$ of civil structures [51]

The following considerations are suggested.

1. Civil structures are clearly multicomponent structures and they can be analysed by means of a one-dimensional CW formulation. In fact, both global and local modes involving columns and floors are correctly detected by LE models.

2. CW models allow us to model the physical surfaces of each structural component. This result is otherwise obtainable only with solid finite elements.

6 Conclusions

This chapter has presented a component-wise approach for the analysis of multicomponent structures. The CW model has been obtained by employing the Carrera unified formulation, which puts at our disposal a very reliable formulation to deal with higher-order beam theories. A number of structures have been considered, including composites, simple and complex aircraft structures, and civil buildings. Static and free vibration analyses have been conducted. The results obtained by means of the CW models have been compared with those from refined TE models, with analytical approaches, and solid and shell finite element models. The proposed CW approach has shown its strength in dealing with several different structural problems. There are several important features to be pointed out.

1. CW models provide three-dimensional solutions.

2. The computational cost of the present beam formulation is considerably lower than those incurred for three-dimensional models.

(a) *Configuration A*, mode 1 (b) *Configuration A*, mode 3 (c) *Configuration A*, mode 4

(d) *Configuration B*, mode 3 (e) *Configuration B*, mode 5 (f) *Configuration B*, mode 9
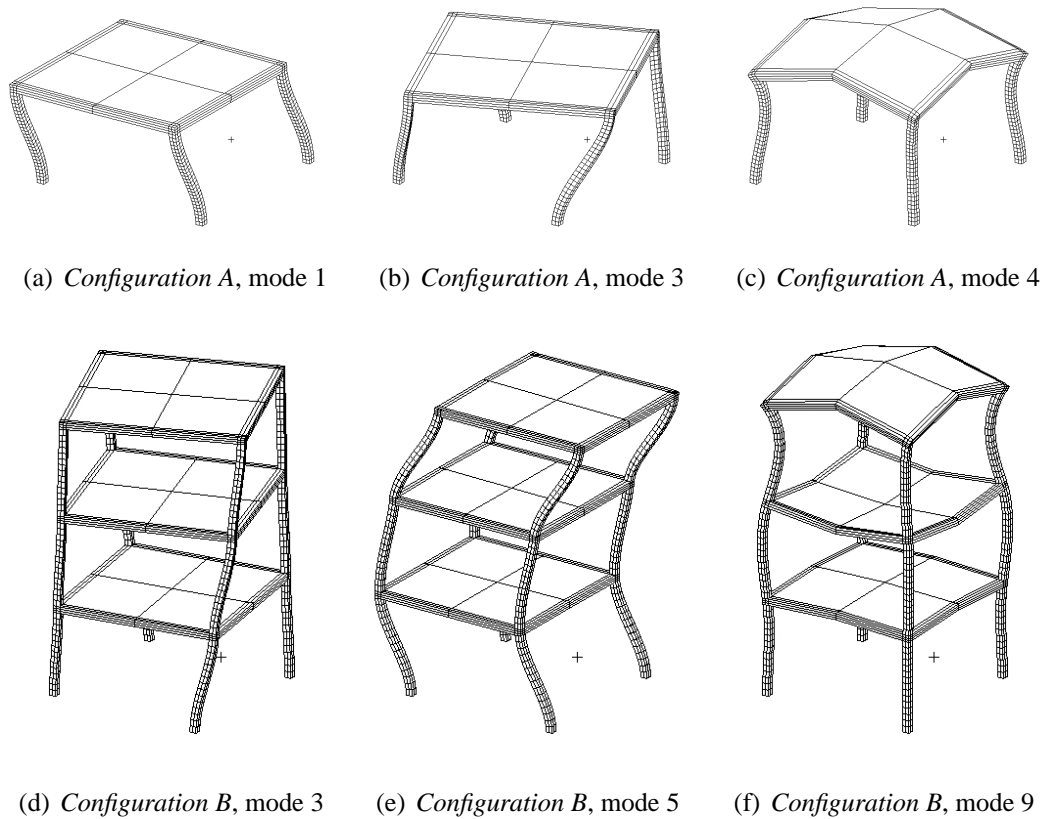
Figure 38: CW modal shapes of civil engineering structures [51]

3. The local refinement offered by Lagrange-based formulations plays a fundamental role in dealing with point loads in the presence of open thin-walled cross-sections.

4. The classical beam constraining approach has been overcome since a three-dimensional distribution of the boundary conditions can be obtained via the present one-dimensional formulation. This implies the possibility of dealing with partially constrained cross-section beams, that is, the possibility of considering boundary conditions which are obtainable by means of plate or shell and solid models only.

5. The proposed CW approach offers significant improvements in detecting the mechanical behavior of laminated structures in particular when stress fields around fibre and matrix cells have to be accurately computed. A global-local approach can be implemented easily since the same stiffness matrix is adopted to model each component of the structure.

6. The present CW analysis appears to the authors to be the most convenient way, in terms of both accuracy and computational costs, to capture the global and lo-

cal (component-wise) physical behavior of multicomponent structures, including aeronautical structures and civil buildings.

7. The CW approach uses only physical surfaces to build FE mathematical models. This characteristic of CW models is a unique feature that gives to this approach clear advantages from a CAE/CAD point of view.

CW should also be employed for failure and damage analysis in future investigations. It is important to underline that the present work deals with linear analysis. However, as far as failure and damage analyses are concerned, nonlinearities - both geometrical and material - can play fundamental roles. The extension of CUF one-dimensional models and CW to nonlinearities should be one of the future tasks to be undertaken. Computational advantages from CUF one-dimensional can be even more evident in a nonlinear scenario where iterative strategies are needed. Moreover, further work should be directed to the development of CW models of fuselage structures and complete aircraft. Transient and gust response analysis will be performed, in the foreseeable future, by means of CW models of wings. Finally, more representative examples of civil structures should be considered. The possibilities offered by CW models could open new scenarios and previously unattainable analysis could be carried out (walls, doors and windows could be included to obtain CW models of complete buildings; soil and foundation analysis could be performed).

References

[1] L. Euler, "De curvis elasticis", Lausanne and Geneva: Bousquet, 1744.

[2] S.P. Timoshenko, "On the corrections for shear of the differential equation for transverse vibrations of prismatic bars", Philosophical Magazine, 41, 744–746, 1921.

[3] S.P. Timoshenko, "On the transverse vibrations of bars of uniform cross section", Philosophical Magazine, 43, 125–131, 1922.

[4] W. Yu, V.V. Volovoi, D.H. Hodges, X. Hong, "Validation of the variational asymptotic beam sectional analysis (VABS)", AIAA Journal, 40, 2105–2113, 2002.

[5] E. Carrera, G. Giunta, M. Petrolo, "Beam Structures: Classical and Advanced Theories", John Wiley & Sons, 2011. doi:10.1002/9781119978565

[6] E. Carrera, M. Petrolo, "Refined beam elements with only displacement variables and plate/shell capabilities", Meccanica, 47(3), 537–556, 2012. doi:10.1007/s11012-011-9466-5

[7] E.F. Bruhn, "Analysis and design of flight vehicle structures", Tri-State Offset Company, 1973.

[8] R.M. Rivello, "Theory and analysis of flight structures", McGraw-Hill, 1969.

[9] E. Carrera, "Fondamenti sul Calcolo di Strutture a Guscio Rinforzato per Veicoli Aerospaziali", Levrotto & Bella, 2011.

[10] S.K. Satsangi, M. Mukhopadhyay, "Finite element state analysis of girder bridges having arbitrary platform", Int. Ass. of Bridge Struct. Engng., 17, 65–94, 1987.

[11] M. Kolli, K. Chandrashekhara, "Finite element analysis of stiffened laminated plates under transverse loading", Composite Science and Technology, 56, 1355–1361, 1996.

[12] T.I. Thinh, N.N. Khoa, "Free Vibration Analysis of Stiffened Laminated Plates Using a New Stiffened Element", Technische Mechanik, 28(3–4), 227–236, 2008.

[13] G.M. Vörös, "A special purpose element for shell-beam systems", Computers and Structures, 29(2), 301–308, 1988.

[14] G.M. Vörös, "Finite element analysis of stiffened plates", Periodica Polytechnica, 51(2), 105–112, 2007.

[15] V.Z. Vlasov, "Thin-walled elastic beams", National Science Foundation, Washington, 1961.

[16] T. Kant, B.S. Manjunath, "Refined theories for composite and sandwich beams with C^0 finite elements", Computers and Structures, 33(3), 755–764, 1989.

[17] K. Kapania, S. Raciti, "Recent Advances in Analysis of Laminated Beams and Plates, Part I: Shear Effects and Buckling", AIAA Journal, 27(7), 923–935, 1989.

[18] S.G. Lekhnitskii, "Strength calculation of composite beams, Vestnik inzhen i tekhnikov, 9, 1935.

[19] S.A. Ambartsumian, "Contributions to the theory of anisotropic layered shells", Applied Mechanics Review, 15, 245–249, 1962.

[20] E. Reissner, "On a certain mixed variational theory and a proposed application", International Journal of Numerical Methods in Engineering, 20, 1366–1368, 1984.

[21] E. Carrera, "Historical review of Zig-Zag theories for multilayered plates and shells", Applied Mechanics Review, 56(3), 287–308, 2003.

[22] D.H. Robbins Jr, J.N. Reddy, "Modeling of thick composites using a layer-wise theory", International Journal of Numerical Methods in Engineering, 36, 655–677, 1993.

[23] E. Carrera, "Evaluation of layer-wise mixed theories for laminated plates analysis", AIAA Journal, 36, 830–839, 1998.

[24] E. Carrera, M. Petrolo, "Refined one-dimensional formulations for laminated structure analysis", AIAA Journal, 50(1), 176–189, 2012. doi:10.2514/1.J051219

[25] H.M. Mourad, T.O. Williams, F.L. Addessio, "Finite element analysis of inelastic laminated plates using a globallocal formulation with delamination", Comput. Methods Appl. Mech. Engrg., 198, 542–554, 2008.

[26] H. Ben Dhia, G. Rateau, "The Arlequin method as a flexible engineering design tool", International Journal of Numerical Methods in Engineering, 62(11), 1442–1462, 2005.

[27] F. Biscani, G. Giunta, S. Belouettar, E. Carrera, H. Hu, "Variable kinematic beam

elements coupled via Arlequin method, Composite Structures, 93(2), 697–708, 2011.

[28] J. Mergheim, "Simulation of Failure Process with the Variational Multiscale Method", International Journal of Material Forming, 2, 899–902, 2009.

[29] J. Fish, "Multiscale Modeling and Simulation of Composite Materials and Structures", Lecture Notes in Applied and Computational Mechanics, 55, 215–231, 2011.

[30] Y.W. Kwon, "Multi-scale modeling of mechanical behavior of polycrystalline materials, Journal of Computer-Aided Materials Design, 11, 43–57, 2004.

[31] J. Aboudi, "Mechanics of Composite Materials: A Unified Micromechanical Approach", Elsevier, 1991.

[32] E.J. Pineda, A.M. Waas, "Multiscale Failure Analysis of Laminated Composite Panels Subjected to Blast Loading Using FEAMAC/Explicit", NASA/TM–2009-215813, 2009.

[33] E.J. Pineda, A.M. Waas, B.A. Bednarcyk, C.S. Collier, P.W. Yarrington, "Progressive damage and failure modeling in notched laminated fiber reinforced composites", International Journal of Fracture, 158(29), 125–143, 2009.

[34] G. Lu, E. Kaxiras, "Handbook of Theoretical and Computational Nanotechnology", American Scientific Publishers, Volume X, 1–33, 2005.

[35] S.W. Tsai, "Composites Design", 4th edn, Dayton, Think Composites, 1988.

[36] J.N. Reddy, "Mechanics of laminated composite plates and shells. Theory and analysis", 2nd edn, CRC Press, 2004.

[37] E. Carrera, G. Giunta, M. Petrolo, "A Modern and Compact Way to Formulate Classical and Advanced Beam Theories", in B.H.V. Topping, J.M. Adam, F.J. Pallarés, R. Bru and M.L. Romero, (Editors), "Developments and Applications in Computational Structures Technology", Saxe-Coburg Publications, Stirlingshire, UK, Chapter 4, 75-112, 2010. doi:10.4203/csets.25.4

[38] E. Carrera, G. Giunta, "Refined beam theories based on Carrera's unified formulation", International Journal of Applied Mechanics, 2(1), 117–143, 2010.

[39] E. Carrera, G. Giunta, P. Nali, M. Petrolo, "Refined beam elements with arbitrary cross-section geometries", Computers and Structures, 88(5–6), 283–293, 2010. doi:10.1016/j.compstruc.2009.11.002

[40] E. Carrera, M. Petrolo, P. Nali, "Unified formulation applied to free vibrations finite element analysis of beams with arbitrary section", Shock and Vibrations, 18(3), 485–502, 2010. doi:10.3233/SAV-2010-0528

[41] E. Carrera, M. Petrolo, "On the effectiveness of higher-order terms in refined beam theories", Journal of Applied Mechanics, 78(2), 2011. doi:10.1115/1.4002207

[42] E. Carrera, M. Petrolo, A. Varello, "Advanced beam formulations for free vibration analysis of conventional and joined wings", Journal of Aerospace Engineering, 25(2), 282–293, 2012. doi:10.1061/(ASCE)AS.1943-5525.0000130

[43] E. Carrera, M. Petrolo, E. Zappino, "Performance of CUF approach to analyze the structural behavior of slender bodies", Journal of Structural Engineering, 138(2), 285–297, 2010. doi:10.1061/(ASCE)ST.1943-541X.0000402

[44] E. Oñate, "Structural Analysis with the Finite Element Method: Linear Statics", Volume 1, Springer, 2009.

[45] K. Bathe, "Finite element procedure, Prentice Hall, 1996.

[46] E. Carrera, M. Maiarú, M. Petrolo, "Component-wise analysis of laminated anisotropic composites", International Journal of Solids and Structures, 49, 1839–1851, 2012. doi:10.1016/j.ijsolstr.2012.03.025

[47] E. Carrera, A. Pagani, M. Petrolo, "Classical, refined and component-wise theories for static analysis of reinforced-shell wing structures", 2012. (Submitted)

[48] E. Carrera, A. Pagani, M. Petrolo, "Component-wise method applied to vibration of wing structures", 2012. (Submitted)

[49] R.J. Allemang, D.L. Brown, "A correlation coefficient for modal vector analysis", Proceedings of the International Modal Analysis Conference, 110–116, 1982.

[50] E. Carrera, E. Zappino, "Static and dynamic response analysis of complex/full aircraft structure by means of advanced one-dimensional models", 2012. (Submitted)

[51] E. Carrera, A. Pagani, M. Petrolo, "Component-wise approach for the analysis of civil engineering structures", 2012. (Submitted)